A METHODOLOGY TO COMPENSATE FOR PART COMPLIANCE DURING ROBOTIC MACHINING

A Dissertation

Presented to

The Academic Faculty

By

Hunter Kim

In Partial Fulfillment

of the Requirements for the Degree

Master of Science in the

School of Mechanical Engineering

College of Engineering

Georgia Institute of Technology

December 2022

A METHODOLOGY TO COMPENSATE FOR PART COMPLIANCE DURING ROBOTIC MACHINING

Thesis committee:

Dr. Shreyes Melkote, Advisor
School of Mechanical Engineering
Georgia Institute of Technology

Dr. Stephen Balakirsky
Georgia Tech Research Institute
Georgia Institute of Technology

Dr. Christopher Saldana
School of Mechanical Engineering
Georgia Institute of Technology

Date approved: December 5, 2022

ACKNOWLEDGEMENTS

I would like to thank all the wonderful people who have supported me throughout my research and the writing of this thesis. First, I would like to thank Dr. Melkote and Allison Brown, who have supported me through my Master's program at Georgia Tech and during my time in the BMDC. I would also like to thank Dr. Melkote, Dr. Balakirsky and Dr. Saldana for their time on my committee. Finally, I would like to thank my parents, Joe Kim and Young Park, for their encouragement throughout my Master's and Mikaela Van Avery, for her never-ending emotional and moral support, motivation and inspiration.

TABLE OF CONTENTS

LIST OF TABLES

LIST OF FIGURES

LIST OF ABBREVIATIONS

ADS Automation Device Specification

CAD Computer Aided Design

CAM Computer Aided Manufacturing

CNC Computer Numerical Control

CSV Comma-separated Values

DOC Depth of Cut

DOF Degree of Freedom

FEA Finite Element Analysis

FEM Finite Element Modeling

HSS High-Speed Steel

IPM Inches per Minute

KRL KUKA Robot Language

PI Proportional Integral

PID Proportional Integral Derivative

RPM Revolutions per Minute

RSI Robot Sensor Interface

SGM Sensor Guided Motion

T-Mac Tracker-Machine control sensor

TiN Titanium Nitride

SUMMARY

Machining thin-walled, compliant parts is a cost-efficient way to manufacture lightweight and structurally sound parts as used extensively in the aerospace industry. Such parts are difficult to machine using traditional CNC machines due to part compliance, increased susceptibility to chatter, and the need for specialized tooling or fixturing devices. These challenges are heightened while machining with a robotic manipulator due to its lower stiffness and easily excited dynamics. However, due to the unique benefits of industrial robotic manipulators such as low cost and a large workspace to footprint ratio, there has been extensive research to maximize the accuracy and path compensation of robotic manipulators. This thesis introduces a methodology to compensate the path of a robotic manipulator to increase the accuracy of peripherally milled compliant parts. The research purpose is to develop an offline path compensation methodology as a solution to the part inaccuracies that occur during machining due to part compliance arising from the forces involved in machining. Two approaches to the compensation methodology are pursued in this thesis. The first approach utilizes experimentally determined dimensional errors to iteratively compensate a nominal path. In the second approach, milling force and part deflection models are used to predict the path compensation needed to compensate the part compliance induced errors. Experiments are performed on a 6-DOF industrial robotic manipulator with a laser-tracker based real-time closed-loop feedback control system. The experiments demonstrate the effectiveness of the iterative robot path compensation strategy in improving part accuracy. The benefits and implications of the compensation strategy are discussed and future improvements to the methodology are recommended.

Chapter 1

Introduction

1.1 Motivation and Problem Statement

Aerospace products such as airplanes involve many thin-walled parts that that need to be machined to within tight tolerances [1]. As modeling and simulation capabilities improve, machining has become faster, more precise, and capable of generating complex structures to maximize part strength to weight ratio. In the aerospace industry, this is evident in the manufacturing of wing ribs and wing boxes, which are characterized by cross-sections of a few millimeters thick that must be manufactured to a tight tolerance as shown in Figure 1.1. Due to the high demand of such parts, they must be machined at the highest feed rates possible while maintaining the part accuracy needed. The design of intricate structures utilizing such thin walls also often creates difficult to machine areas due to limited tool clearances and angled structural parts. Traditional machining utilizing monument-type gantry Computer Numerical Controlled (CNC) milling machines are often used in the aerospace industry due to their high accuracy and material removal rates. However, their high cost, large machine footprint, and lack of flexibility in constantly evolving production lines have spurred research into articulated arm robots, which offer a large workspace to footprint ratio, significantly lower costs, and high machining flexibility. The cost of these benefits lies in decreased path accuracy due, in large part, to the lower stiffness and kinematic accuracy of articulated arm robots, especially for machining thin-walled parts.

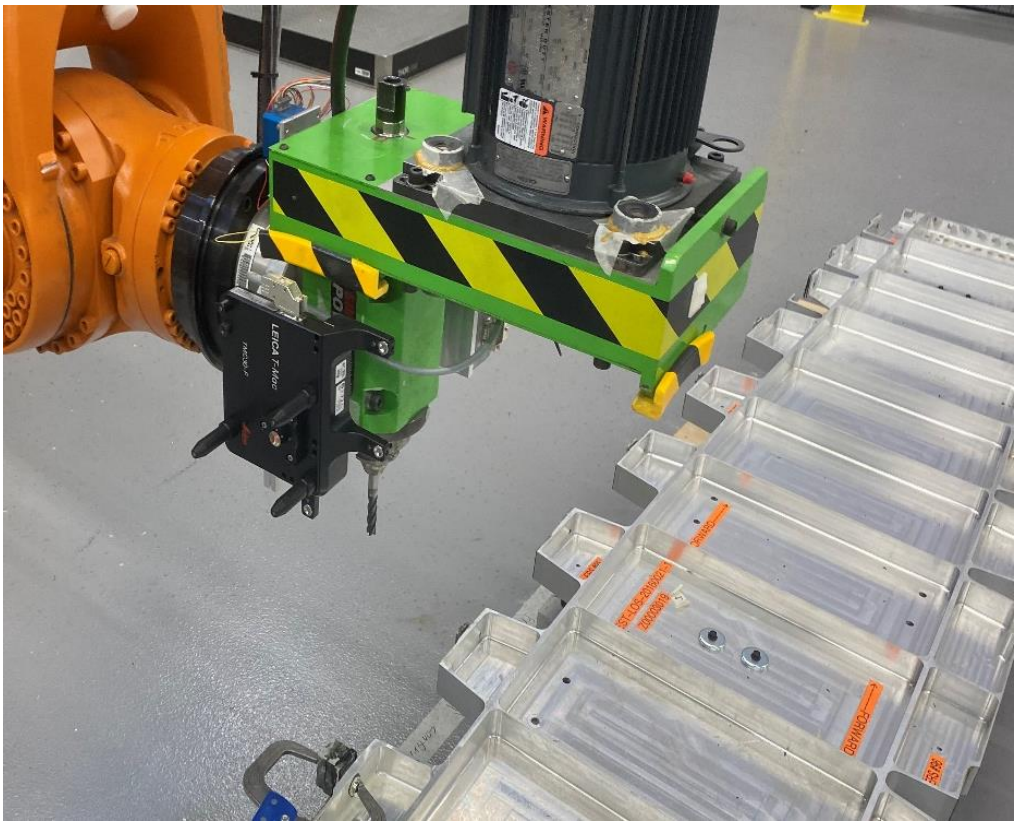

Figure 1.1: Aerospace wing rib with CNC machined thin-walled regions

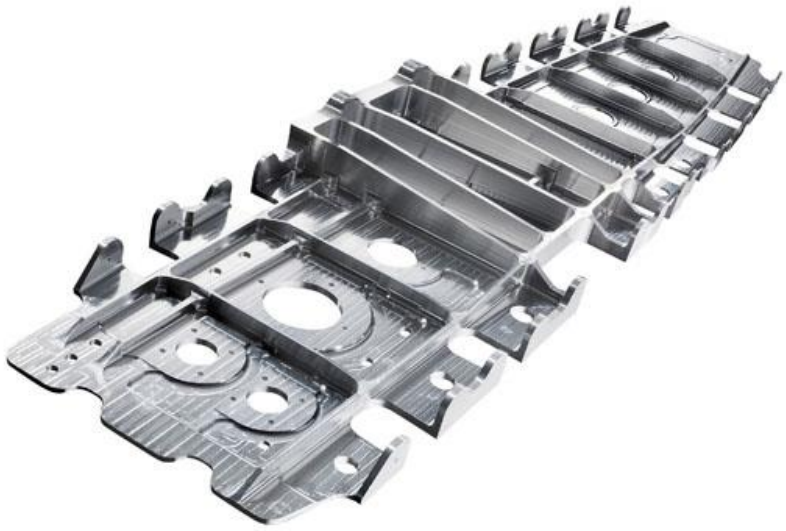

Figure 1.2: Complex geometries used for aerospace parts driven by weight savings [2]

Six degree of freedom (6DOF) robots are capable of a high degree of versatility in terms of tooltip position and orientation control only seen on the highest end traditional CNC machine tools. Additionally, the robotic arm's workspace is significantly larger than its footprint while CNC machine tools rely on working entirely within a relatively small portion of their overall footprint. Inherently, this causes articulated robot arms to have a lower stiffness, which makes them on the order of magnitude of 50 times more compliant [3, 4]. This has led to research in real-time online robotic arm path compensation to correct their position to within 0.1 mm [5]. However, real time path compensation strategies are often expensive due to the high-fidelity laser trackers and precisely calibrated control software required for implementation. Thus, an offline path compensation strategy is desired which can supply the benefits of path compensation without the high cost of metrology capabilities needed for online compensation methods. Such an offline path compensation strategy also offers the benefit of the utilization of complex models for path compensation, which generally cannot be evaluated in real time to enable control. An offline path compensation strategy could also be utilized for traditional CNC machines in addition to robotic arm manipulators, increasing the relevancy of the method.

Using real time feedback robotic manipulators have been shown to be capable of up to 0.1 mm path accuracy [5]. However, this does not accurately demonstrate the machining accuracy of the robot for thin-walled parts since the part deflects significantly due to the high forces involved in machining, which leads to decreased part accuracy. The key aspects of thin-walled machining contributing to the decreased part accuracy are part deflections, part geometric errors, and fixturing errors. To compensate for these part errors using real-time robot position and orientation feedback, the part *and* the robot would need

to be tracked by suitable sensors (e.g., 6DOF laser tracker), which is an impractical method due to cost and system feedback complexity.

Current CNC machine tools can compensate for thin-walled parts using a variety of methods including multiple small depths of cut to decrease the forces generated during machining, artificially increasing the stiffness of the part through use of stiffeners or complex fixturing solutions, and reduced feed rates to decrease the milling forces generated [6-8]. These methods are effective, but each have drawbacks resulting in decreased production rates or costly specialized fixturing/tooling. In addition, data driven models rely on large amount of data and are not robust in extrapolation due to the complex dynamics involved in machining [9]. A model-based approach is preferred to utilize the system and machining information available to accurately predict the necessary robot tool tip path compensation without the need for large robot downtime arising from data sampling or expensive sacrificial parts. This demonstrates the need for alternate methods to compensate for path accuracy errors through the use of offline path compensation determined through modeling and simulation of part errors due to part-fixture compliance, etc.

The challenge of machining compliant, thin-walled parts with CNC machines and robotic manipulators poses a hurdle for the aerospace industry. Current strategies to achieve high part accuracy for thin-walled machined parts have clear drawbacks in diminished production speeds or higher cost, which are key considerations for the aerospace industry [10]. This thesis addresses the challenge of machining thin-walled parts using a 6DOF industrial robot to enable a lower cost and flexible machining solution capable of delivering the required part accuracies for aerospace applications. Specifically, the thesis presents an offline robot path compensation strategy that is capable of accounting

for part-fixture compliance and other potential error sources. Both pure data-driven and model-based predictive approaches are developed and evaluated through robotic milling experiments.

1.2 Research Objectives

Driven by the problem statement, the objective of this research is to develop a novel predictive off-line path compensation strategy to account for part deflections due to cutting forces. A real time laser tracker is used to verify path accuracy and the part is measured after machining to determine part accuracy. The objective is broken down into the following parts:

1. Develop a compensation strategy to reduce part errors due to part compliance based on experimental data.
2. Utilize machining models incorporating part deflection and machining forces to create a purely model based compensation approach.
3. Perform model-based compensation and compare results with experimental compensation results to assess part accuracy improvements.

1.3 Proposed Approach

To achieve the listed research objectives, the following approach was followed. First, the effect of part compliance during robotic milling of a thin-walled aluminum workpiece is investigated, yielding a purely data-driven model that serves as the basis for an initial compensation strategy. This data-driven model along with robot repeatability guarantees that changes in part accuracy are due to the compensation strategy and not due to varying experimental conditions or modeling assumptions. The offline compensation

strategy uses the data-driven model to alter the robot's path to increase the effective depth of cut. This data-driven compensation strategy is then validated through assessment of the final machined part accuracy and through comparison with the non-compensated experimental results. Using the same methodology, a purely model-based compensation strategy is explored through Finite Element Analysis (FEA) of thin-walled part deflections and a mechanistic milling force model for the machining forces. Combined, these two models yield the expected deflection of a given thin-walled part for a known set of machining conditions. The value of this model lies in the complete elimination of experimental calibration required for the data-driven compensation strategy. The effectiveness of the model-based compensation strategy is then assessed through comparison with part accuracy of the non-compensated and data-driven compensated trajectories. Next, the model is further expanded by considering the effect of part deflection on the machining forces. This effect compounds on itself as machining forces impacts part deflection which in turn impacts the machining forces. Finally, this compliant model-based compensation strategy is tested and the resulting part accuracy is evaluated relative to the other methods. This approach is summarized in Figure 1.3.

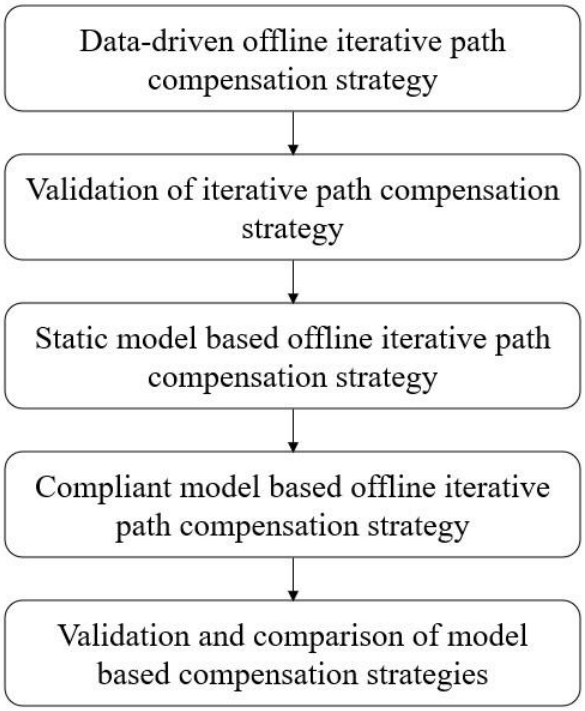

Figure 1.3: Summary of approach.

1.4 Thesis Outline

The thesis is organized in the following order.

Chapter 2 reviews prior works and the recent state of the art in robotic machining and offline path compensation. Chapter 3 introduces the iterative path compensation strategy for peripheral cuts and discusses the experimental procedure used for compensation validation. Chapter 4 builds upon the compensation strategy using a modeling approach to eliminate the need for experimental calibration. Rigid and compliant models are used to assess the performance of the model-based compensation strategy and to eliminate part form errors such as tapering of the peripherally milled wall. Chapter 5 concludes the thesis by drawing the main conclusions of the work and recommending areas for future work.

CHAPTER 2

LITERATURE REVIEW

This chapter presents a literature review to understand the state of the art of robotic machining path compensation and relevant research objectives. The review will cover the following three sections: 1) path compensation in CNC machines, 2) path compensation in traditional robots, 3) error compensation for machining of thin-walled parts.

2.1 Path Compensation in CNC Machines

The industry standard machining tool is a CNC machine, a computer numerical control machine due to their high stiffness characteristics, path repeatability, and high accuracy. CNC machines are also often used to machine thin-walled parts and there are various compensation methods for such machining scenarios. Although these compensation methods may be effective for CNC machines, it should be noted that such path compensation may not necessarily work as effectively on an industrial robot due to the increased compliance of the robot. Path compensation that relies on the high stiffness of the machine tool then must be carefully assessed before application in a robotic machining environment.

As CNC machines have a high degree of precision, machined part geometrical and dimensional inaccuracies can be attributed to workpiece and tool deflection, thermal distortion, tool wear and machine tool inaccuracies. Machined part inaccuracies can be reduced through the comparison of the initial CAD model used for computer aided machining and the machined part. The CAD model can then be adjusted based on the

discrepancies between the desired part and the final product [11]. This method relies on the high repeatability of CNC machines as well as the predictability of the workpiece which may not be directly applicable for robotic machining as the robot is significantly less stiff and can have pose dependent stiffness characteristics [12].

Another area of interest is path compensation in addition to vibration avoidance as severe vibrations of the machining system can lead to chatter and decreased machined part surface accuracy. The path compensation for machining vibrations and contour errors can be mapped to locations along the robot path inputs. This creates a path and CNC machining drive dependent compensation strategy [13]. Additional approaches further investigate the translational and orientational errors of the CNC machine servo drives for compensation which has proven to significantly improve machined part accuracy [14, 15]. Inertial and damping limitations of the machine axis can be accounted for as well using a dynamics model of the machine [16]. Path dependent compensation strategies can be simple to implement as compared to active compensation strategies with an increased emphasis on system modeling. These methods depend on modeling of the physical systems involved in machining as well as the machining trajectory to create an effective compensation strategy. This methodology of system modeling can be highly effective if the system is well defined and predictable.

CNC machining path compensation strategies utilize the known characteristics of the machine in order to reliably determine the error. This methodology can be time consuming as the usage of experimental results to path compensate requires several machining runs and the results of a given compensation cannot be applied to similar cuts due to the potential variations in generated trajectory. On the other hand, system modeling

can be effective in error prediction and compensation as CNC machining is high repeatable. The modelled system is used to generate a path dependent compensation for each machining axis. Industrial robotic machining systems can be more difficult to model due to increased susceptibility to vibrations and chatter as well as the need for both pose and path dependent compensation [17]. As a result, traditional robots require more care when developing system models or alternative compensation strategies.

2.2 Path Compensation in Traditional Robots

Industrial robots have been utilized in various fields boasting a high range of motion and maneuverability due to their 6DOF control. Robots are now commonly seen in medical, manufacturing, and warehousing applications [18 – 21]. For manufacturing applications, the precision required can exceed the off-the-shelf accuracy limitations of industrial robots as Kuka industrial robots have an experimental maximum absolute positional error of 1.53 mm [22]. This maximum positional error is an order of magnitude higher than the 0.1 mm positional accuracy desired by aerospace applications, creating the need for path compensation even before a part is being machined. In comparison, a CNC machine can have maximum positional accuracy errors on the order of magnitude of 0.005 mm, well within the tolerances desired for aerospace applications [23]. During machining conditions, the maximum positional error increases due to the machining forces combined with the low stiffness of the robotic arm compared to CNC machines [24].

Path compensation strategies include offline path compensation through the use of robot compliance modeling and cutting forces predicted by mechanistic models. The path is compensated through modified trajectory G-code using static tooltip displacement calculations. Results demonstrated a significant decrease in machined part surface errors

through the method to compensate for robot deflection [24]. Similar studies explore the use of joint compliance and hysteresis models to compensate for reversal errors for similarly considerable reduction in part surface errors [25]. Thus, a proven effective method for path compensation of industrial robotic arms in machining applications is a creation of a system model to determine the expected path errors which are then compensated. However, these methods equate the magnitude of path compensation to the modelled error which assumes that path compensation will not impact the magnitude of error that was modelled. For small errors, this assumption may be viable as the modelled error will not increase significantly due to the changes in the system variables, but may change as the modelled errors increase.

2.3 Error Compensation for Machining of Thin-Walled Parts

During machining of thin-walled parts, there can be significant temporary deformation of the thin-wall as the machining forces are applied on the machining surface. This results in the both machined part surface errors as well as decreased machining forces both due to decreased depth of cut [26, 27]. For CNC machining, a solution for machining of thin-walled parts is to determine the error due to compliance and compensate the tool path similar to robotic arm compliance compensation discussed previously. This solution offers a method to predict the compliance of one component of the machining system due to its relatively low stiffness [28]. Another consideration during the machining of thin-walled structures is the possibility of chatter. As the part deflects relative to the cutting tool and vibrated due to the cyclical machining forces, chatter is created. Chatter can be reduced through a time-varying dynamic system model with the magnitude of chatter vibrations determined through static and dynamic material stiffness at a given instant in time [29].

However, chatter is an avoidable artifact of a compliant system and can be eliminated through careful selection of machining feed rates and spindle speeds. Although some studies exist in path compensation during machining of compliant thin-walled parts, current strategies for machining thin-walled structures involve avoiding the issue of compliance rather than decreasing the induced error. As a result, industry machining of thin-walled structures involves usage of lubricants to decreasing thermal effects and machining forces and damping attachments made of rubber, clay or a tuned mass to attach to the thin-wall structure [30]. Beyond these methods, careful adjustment of the feeds and speeds are sufficient to completely eliminate chatter. For the purposes of the path compensation strategy discussed in this thesis, the effect of chatter is not considered as the machining conditions used do not create chatter.

CHAPTER 3

DATA-DRIVEN MODELING AND ITERATIVE PATH COMPENSATION STRATEGY FOR PERIPHERAL MILLING

3.1 Introduction

Path compensation is a simple yet effective concept for eliminating error in a desired path. Existing research on path compensation focuses on correcting desired tooltip paths due to robotic arm compliance or robot kinematic errors, however, part compliance and fixturing errors can play an equally important role in determining the accuracy of the robotic milling operation [31]. Compensation strategies can function either online or offline, with offline compensation strategies offering straightforward application and development while online compensation strategies are more robust and can account for errors that are not modelled. The objective of this chapter is to study the part errors occurring during machining of thin-walled parts using a 6DOF articulated arm robot and develop a compensation strategy using a data driven model. Part errors can mainly be attributed to fixturing, part surface geometry, or part compliance errors, of which part compliance is the most significant during machining of thin-walled parts. In addition, despite articulated robotic arms having lower stiffness than traditional CNC machines, part errors are dominated by part compliance due to the exponential decrease in part stiffness with decreasing wall thickness. Plate stiffness is proportional to its bending moment of inertia which is proportional to the plate thickness to the third power [32]. In this chapter, fixturing and surface geometry errors are minimized to ensure part errors can primarily be attributed to part deflection in the presence of machining forces. First, the non-

compensated robot trajectory for a peripheral milling cut is run to determine a baseline for part error given varying wall thicknesses. The part errors are then analyzed to develop a suitable data-driven compensation strategy. The data driven compensation strategy is used to predict a static offset to the robot path to compensate for part compliance. The proposed data-driven part compliance induced machining error compensation strategy is experimentally assessed for its effectiveness.

3.2 Overview of Compensation Method

This section describes the compensation methodology and the assumptions used to develop the data-driven compensation model. The robotic milling system is defined to consist of the 6DOF articulated robotic end effector and the part being machined. To isolate the part geometry errors due to part compliance, the part errors due to the robot must first be accounted for. This is done through the use of a laser tracker providing 6DOF positional corrections to the robot end effector. The utilization of the laser tracker ensures that the programmed trajectory is followed by the robot within 0.1mm accuracy and ensures that any part errors due to the robot path is less than 0.1mm. Next, part errors due to fixturing must be minimized which can include inconsistent or loose fixturing. This can be eliminated by situating the part in a secure floor mounted vice with no movement between tests, effectively eliminating fixturing part errors. Lastly, the part errors due to geometry errors include surface irregularities on the part and material non-homogeneity, which can be minimized through the use of solid aluminum that has been planed before every test.

Thus, through these methods, it is ensured that any remaining part surface errors are primarily due to the compliance of the part with minimal impact from unaccounted or reduced error sources. This leads to the assumption that any part dimensional errors after

machining are solely due to part compliance. This ensures that the methodology for compensation can be developed to eliminate all part errors that are observed without accounting for additional errors sources. Using this assumption, a methodology can be created to compensate the robot end effector trajectory to eliminate any errors determined experimentally using a data driven model. Considered sources of part error are shown in Equation 3.1.

$$P_{Comp} = f(\varepsilon) + P_{Nom}$$
$$\varepsilon = \varepsilon_{work} + \varepsilon_{fixture} + \varepsilon_{compliance} + \varepsilon_{tool} \quad (3.1)$$

P_{Nom} = Nominal path

P_{Comp} = Compensated path

ε = total errors for a given path

3.3 Iterative Path Compensation Strategy

Given the aforementioned system, it is clear that non-compensated trajectories will result in part errors due to part compliance despite nominally accurate end effector movement. An intuitive solution to compensate for this compliance is to provide a static offset as path compensation as shown in Figure 3.1. This static path compensation can easily be programmed as an increased radial depth of cut for a peripheral milling operation. However, a static offset is insufficient to provide full path compensation as increasing the radial depth of cut increases the cutting forces involved in machining, which in turn increases the deflection of the part. In addition, the initial conditions of the cut are altered, diminishing the potential of a single non-compensated cut to be utilized for path compensation.

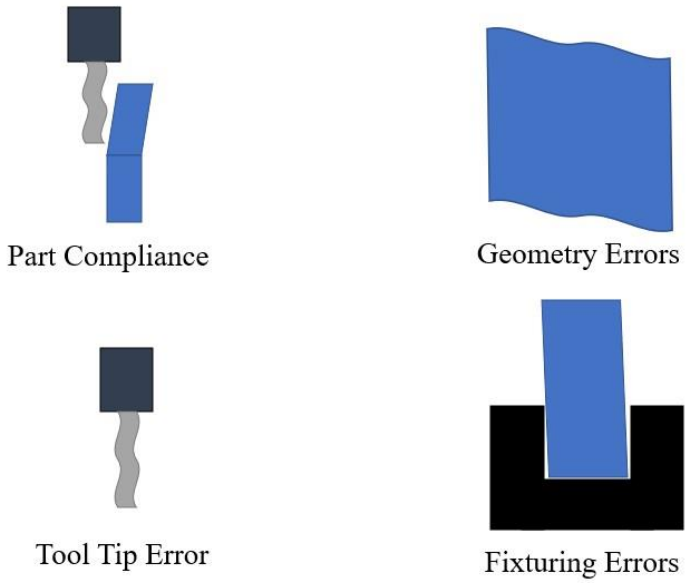

Figure 3.1: All part error sources.

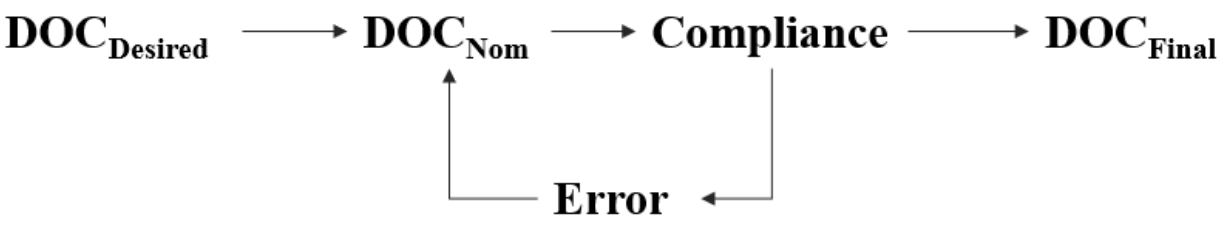

Figure 3.2: Iterative compensation method.

As a result, a more robust compensation strategy is developed using an iterative procedure to predict the increase in radial depth of cut due to path compensation as shown in Figure 3.2. Given an initial, desired radial depth of cut, $DOC_{Desired}$, there is a corresponding nominal radial depth of cut, DOC_{Nom} which have the same value in the first iteration. However, the DOC_{Nom} causes part deflection, which is reflected in part dimensional accuracy error, *Error*. Utilizing this error as feedback, the DOC_{Nom} is increased by adding the *Error* to the previous DOC_{Nom}, which leads to increased part

deflection and an additional *Error* term. As the *DOC* is increased by the amount of *Error*, this additional *DOC* will also result in *Error* by a given amount. This iterative cycle is repeated resulting in the DOC_{Nom} converging to a DOC_{Final} as the additional *Error* approaches zero. This iterative computation can be represented as the sum of a geometric series, which can be determined algebraically to determine the DOC_{Final} based on a single *Error* value for a given $DOC_{Desired}$. The geometric series equations are shown in Equation 3.2 and a visual representation of the converging geometric series in Figure 3.3 over 7 iterations.

$$\textit{Expanded Compensation: Error} + Error^2 + Error^3 + \ldots$$

$$Iterative\ Compensation = \sum_{i=1}^{\infty} \boldsymbol{\varepsilon}^i \qquad 3.2$$

$$Where\ \ \boldsymbol{\varepsilon} = Compliance\ Error\ Fraction$$

$$\textit{Geometric Series: } \boldsymbol{f}(\boldsymbol{\varepsilon}) = \frac{1}{1-\boldsymbol{\varepsilon}}$$

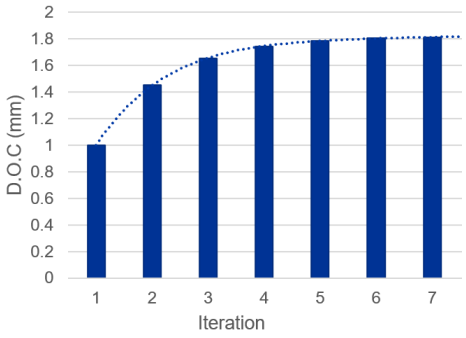

Figure 3.3: Visualization of the convergence of the iterative radial depth of cut computation method for an assumed initial radial depth of cut error of 44%.

In order to utilize this iterative method, two assumptions are made regarding the machining forces:

1. The increase in radial depth of cut error for a given nominal depth of cut is a constant fraction of the increase in the DOC.
2. The compliance of the part does not impact the cutting forces.

An assumption is made that the milling forces do not change with increasing DOC in each iteration. This ensures that the *Error* due to the DOC_{Nom} will remain a static proportion, thus resulting in a geometric series. This assumption is reasonable when the increase in the DOC_{Nom} with each subsequent iteration is sufficiently small. Cutting forces generated in machining aluminum are high at production machining rates and given a small compliance and small error, the increase in the milling forces should be small as well. Furthermore, there is one additional assumption being made regarding the milling forces. As a compliant part is being machined, in reality the machining forces acting on the compliant part cause the part to deflect away from the tool, thereby resulting in removal of less than the nominal radial depth of cut. Consequently, the actual milling force is lowered. However, this effect is not considered in developing the iterative radial depth of cut compensation method presented in this chapter. . Complete elimination of the part error through the use of this iterative method would demonstrate that the combination of the two assumptions is valid for the given model.

3.4 Robotic Milling Experimental Setup

The experimental setup used in this thesis comprises of a 6DOF articulated robotic arm, a laser tracker for positional feedback, a milling spindle, and a floor mounted vice and workpiece as shown in Figure 3.4 and Figure 3.5. The robotic arm is a KUKA KR500-3, which has maximum load capacity of 500 kg, reach of 2825 mm and pose repeatability of 0.08 mm. Attached to the end effector flange is the milling spindle (Suhner Max 40B). The spindle has a maximum torque of 400 Nm, maximum power of 7.5 kW and a spindle speed range of 500-6000 rpm.

The robot positional feedback control loop comprises of a calibrated Leica AT960 laser tracker and a Leica T-Mac TMC30-F tracker-machine control sensor. The T-Mac is securely mounted to the robot spindle and is continuously measured by the laser tracker to determine its 6DOF position and orientation. As the T-Mac is rigidly connected to the spindle and robot end effector, a constant frame shift is applied to the laser tracker measurements to determine the 6DOF position and orientation of the end mill. The Leica laser tracker and T-Mac system has a positional accuracy of ±15 µm + 6 µm/m and a rotational accuracy of ±0.01° with measurements taken at a frequency of 1 kHz. At a distance of 3 meters, the total positional accuracy is ±33 µm.

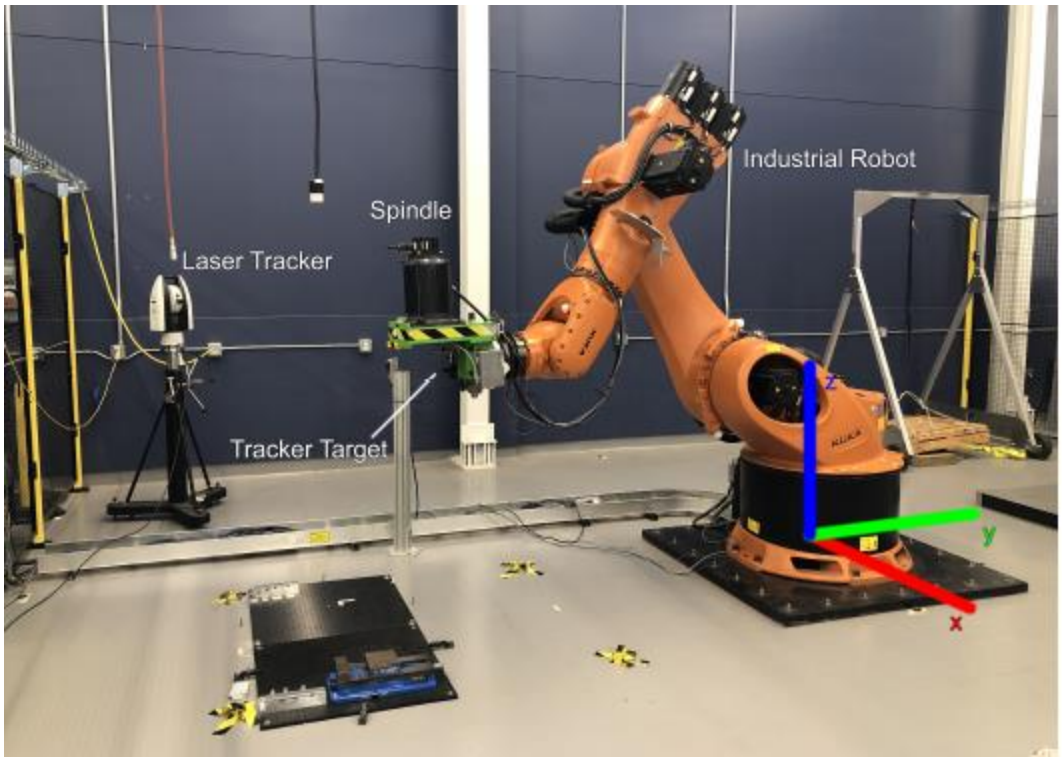

Figure 3.4: Experimental robotic milling system

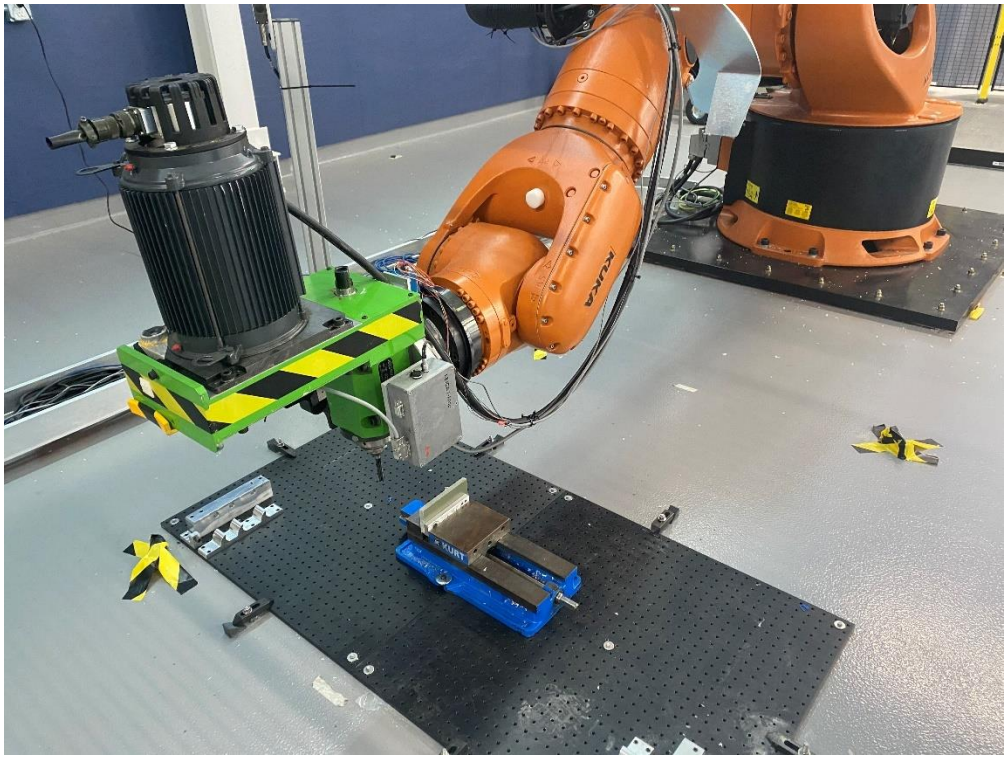

Figure 3.5: KR500-3 Robot with workpiece setup

KUKA provides an option to control the robot using the KUKA Robot Language (KRL) via the KUKA robot controller (KRC4). This enables the user to provide the robot with information for the planned path, which is determined by the robot controller using a built-in path planning algorithm, with the ability to send real-time path corrections through the Robot Sensor Interface (RSI) feature provided by KUKA. To maximize control of robot position through real-time external metrology feedback (and therefore minimize interference by the native robot controller), such as through the laser tracker, this thesis utilizes a real-time robot position control approach termed here as Sensor Guided Motion (SGM) where all movements of the robot are controlled by an external program that feeds cartesian position commands to the KRC4 through RSI. For SGM, a point-to-point path is created to define the trajectory that will be followed. The path files are generated as a nominal desired path along with a static offset for path error compensation. Once the path is run, the laser tracker 6DOF measurements are relayed to a control Windows computer running a real-time control environment (TwinCAT from Beckhoff Automation) using the EtherCAT protocol. The feedback control algorithm is run in the TwinCAT environment and uses proportional-integral-derivative (PID) control to send corrections to the KUKA robot in real time. The PID system command cycle time from laser tracker measurement to robotic arm correction is 4 ms ensuring smooth and rapid corrections. Every command cycle, the laser tracker measures the T-Mac position and orientation and sends this information to the TwinCAT program, which then computes the corrections needed using a PID controller. The PID control gains used in the experiments reported here were proportional gain K_P of 0.05, integral gain K_I of 0.3, and derivative gain K_D of 0.00. The TwinCAT program uses calibrated transformation matrices to locate the end mill with

respect to the robot's calibrated cartesian base frame and computes corrections to meet the preprogrammed desired path. The computed trajectory corrections are given to the robot via KUKA RSI which are then converted into robot joint configurations by the KUKA robot controller.

The workpiece used in the experiments is a 6.35 mm thick, 50 mm wide, 100 mm tall coupon of 6061-T6 aluminum. The workpiece thickness is used as the control variable in the experiments to evaluate the performance of the iterative depth of cut error compensation method as a function of increased part compliance. Specifically, workpiece thickness is decreased from 6 mm to 3 mm in 1 mm decrements to enhance part compliance effects. . The milling process parameters consisted of a linear climb milling peripheral cut of 1 mm radial depth and 35 mm axial depth along the entire 50 mm width of the workpiece using a 4 flute, 25.4 mm diameter, TiN coated HSS square end mill (McMaster 8919A56). The spindle speed was 1000 RPM for all experiments. For planing cuts, a feed rate of 41 mm per minute was used to ensure a flat and smooth initial workpiece surface. For experiments a faster 82 mm per minute feed rate was used. These feeds and speeds yield a feed per tooth of 0.2 mm and 0.4 for planing and cutting respectively. The workpiece is fixed in a mechanical vise such that 40 mm of material protrudes above the clamp resulting in a 50 mm wide 45 mm tall plate. This simulates a thin-walled plate workpiece with three free edges and one fixed edge. The workpiece setup is shown below in Figure 3.6.

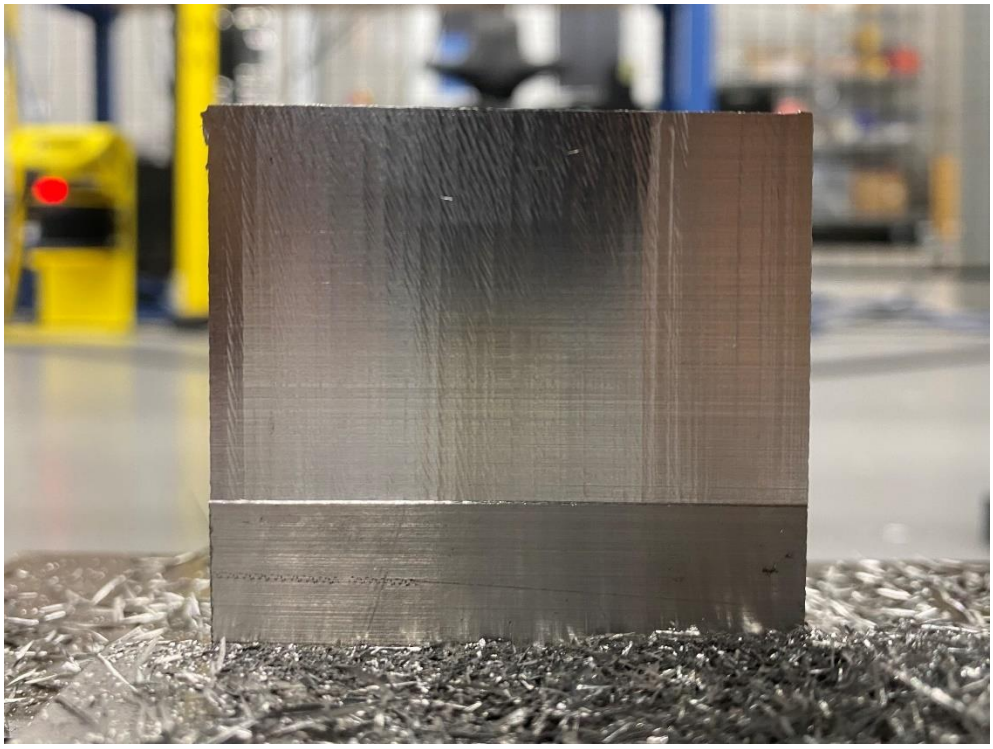

Figure 3.6: Workpiece after peripheral milling using a mechanical vise fixture

3.5 Validation of Iterative Compensation Method

For testing and validation of the iterative compensation methodology presented earlier, two sets of experiments were run: non-compensated trajectories and data-driven iteratively compensated trajectories. The results of tests conducted using the non-compensated trajectories give a baseline part error that can be compared to part errors obtained when using the iteratively compensated trajectories. The part errors of the non-compensated trajectories also serve as the inputs to the iterative compensation methodology, which, as described earlier, require knowledge of the part compliance induced radial depth of cut error (as a fraction of the nominal radial depth of cut) as input to the iterative radial depth of cut compensation computation procedure. The controlled variable was the cut part wall thickness, allowing the part compliance induced depth of cut error to be experimentally determined as a function of the nominal radial depth of cut. First

the non-compensated trajectories were run according to Table 3.1. A planing cut was first run on the surface of the part to ensure no part geometry errors can impact the path or cutting forces. Then, the robot was programmed to perform linear peripheral milling passes with a 1 mm nominal radial depth of cut and the machined part error was determined from analysis of the Leica T-Scan measurements of the planed and cut surfaces. The workpiece setup used in these experiments is shown in Figure 3.7.

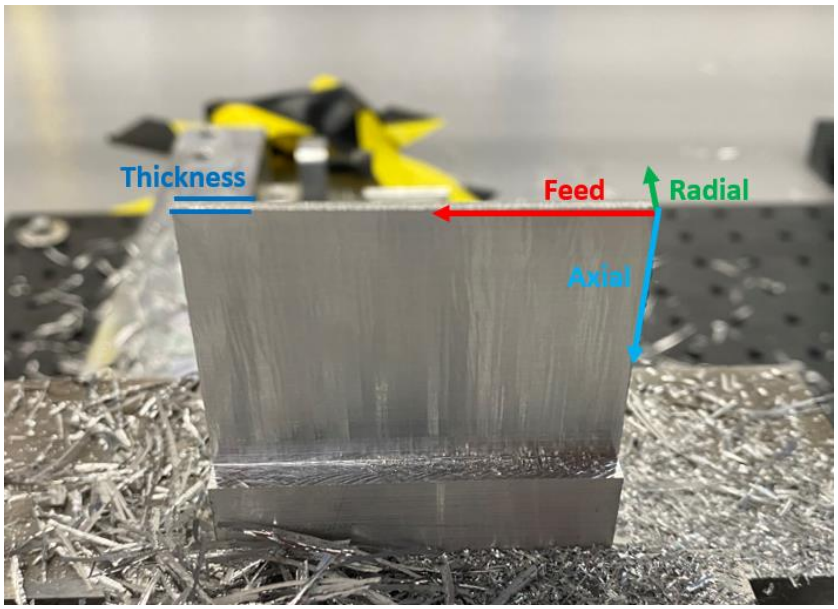

Figure 3.7: Workpiece for peripheral cuts

3.5.1 Non-Compensated Peripheral Cut

For a baseline of non-compensated robotic machining part accuracy, the desired path is used with no path compensation. This provides a baseline error for the iterative compensation strategy as discussed above. Using the setup described previously, the part was planed to varying starting thicknesses from 6, 5, 4, to 3 mm, allowing for a controlled and repeatable decrease in part stiffness. Then, the part was peripherally milled with 1 mm radial depth of cut and 35 mm axial depth of cut. The milled surface was measured using a Lecia T-Scan that generated a cloud of points, which was processed in the Spatial

Analyzer software to fit least squares planes that enabled the mean radial depth of cut errors for the different test cases. Representative views of the cloud point measurements of the planed and milled surfaces for a 4 mm experiment are displayed in Figure 3.8 and Figure 3.9, respectively. Mean planes were fit to the point cloud measurements for the planed and milled surfaces using the least squares method. Due to the mean plane fitting, an RMS error is associated with each measurement with an average of ±0.0262 mm corresponding to the measurement precision of the Leica T-Scan of ±0.032 mm. The distance between the planed and cut mean planes yielded the actual radial depth of cut obtained in the experiments. The difference between the nominal and the actual radial depth of cut represents the radial depth of cut error in each experiment.

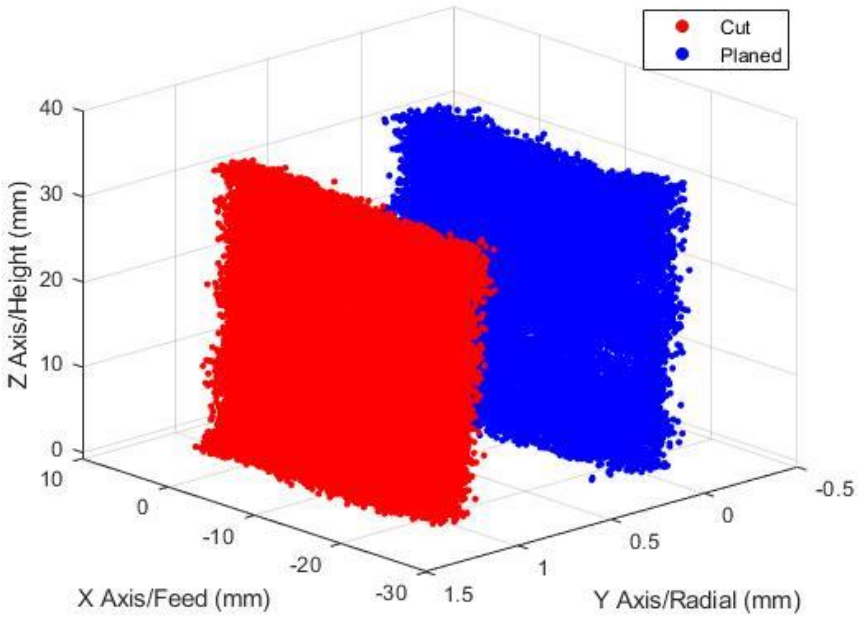

Figure 3.8: Point cloud measurements of the planed and milled surfaces obtained from Leica T-Scan measurements.

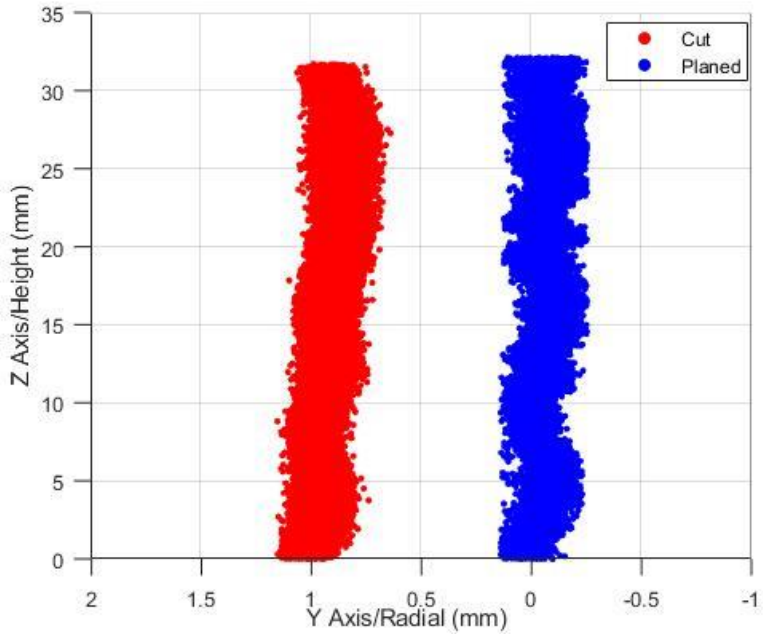

Figure 3.9: Side view of the point clouds of the planed and milled surfaces

It is noted that due to the averaging method used to determine the locations of the measured planes, there is a loss of information related to the specific trends in radial DOC with respect to the Z and X axes. These effects are discussed in Section 5.3 of the thesis.

3.5.2 Non-Compensated Cut Results

Table 3.1: Measured part errors for non-compensated cuts

Starting Part Thickness (mm)	Nominal Depth of Cut (mm)	Measured Part Thickness Error (mm)
6	1	0.15
5	1	0.17
4	1	0.22
3	1	0.27

The resulting part wall thickness errors ranged from 0.15 mm to 0.27 mm signifying a 15-27 % error in the actual radial DOC. The part error is observed to increase as the starting part thickness decreases. This inverse relation stems from increased part compliance of thinner walled parts. The cutting tool produces a force at each point of contact with the workpiece causing a deflection at the point of force application. The result is a decrease in the actual radial depth of cut as the workpiece elastically deflects away from the cutter during milling and returns to the original position after machining.

An interesting workpiece characteristic is seen in the measured part errors. The measured part error for the 5 mm thick workpiece is 0.02 mm higher than for the 6 mm workpiece. In comparison, the 4 mm workpiece error is 0.05 mm higher than for the 3 mm workpiece. This effect can be explained as workpiece stiffness is a cubic function of its thickness as seen experimentally through the non-linear increase in measured part error. However, the experimental results do not strictly follow a cubic increase as the difference in consecutive measured part errors is 0.02 mm, 0.05 mm, and 0.05 mm, respectively. This suggests that there are additional factors besides part thickness that are impacting the final part error.

3.5.3 Data Driven, Iteratively Compensated Peripheral Cuts

The compensated radial depths of cut for each nominal wall thickness case were determined using the iterative compensation method presented earlier. The part compliance error fraction used in the iterative method for each wall thickness was derived from the measured part error obtained in the corresponding non-compensated trajectory experiment. The compensated radial depths of cut for the different experiments are as shown in Table 3.2.

Table 3.2: Compensated radial depths of cut using data-driven model

Nominal Part Thickness (mm)	Compliance Error Fraction (%)	Compensated Radial Depth of Cut (mm)
6	15	1.16
5	17	1.20
4	22	1.28
3	27	1.37

. To apply the path compensation, the articulated arm robot was programmed to cut at the new radial depths of cut instead of a constant 1 mm radial depth of cut. It is noted that the compensation ranges from 16 % for the 6 mm workpiece to 37 % for the 3 mm workpiece. The 3 mm workpiece deflected significantly during the non-compensated experiment and therefore has a substantially increased nominal depth of cut after compensation.

3.5.4 Compensation Strategy Results and Analysis

Similar to the non-compensated experiments, the point cloud measurements of the planed and milled surfaces shown in Figures 3.10 and 3.11 were used to determine the best fit planes. It can be seen that the milled surface is significantly closer to the desired nominal radial depth of cut of 1 mm.

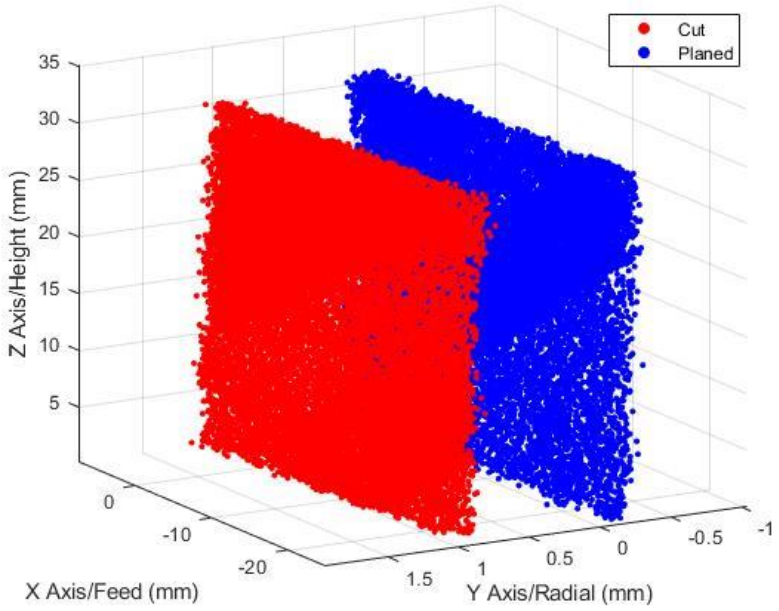

Figure 3.10. Point clouds of the milled and planed surfaces measurements of 4 mm plate.

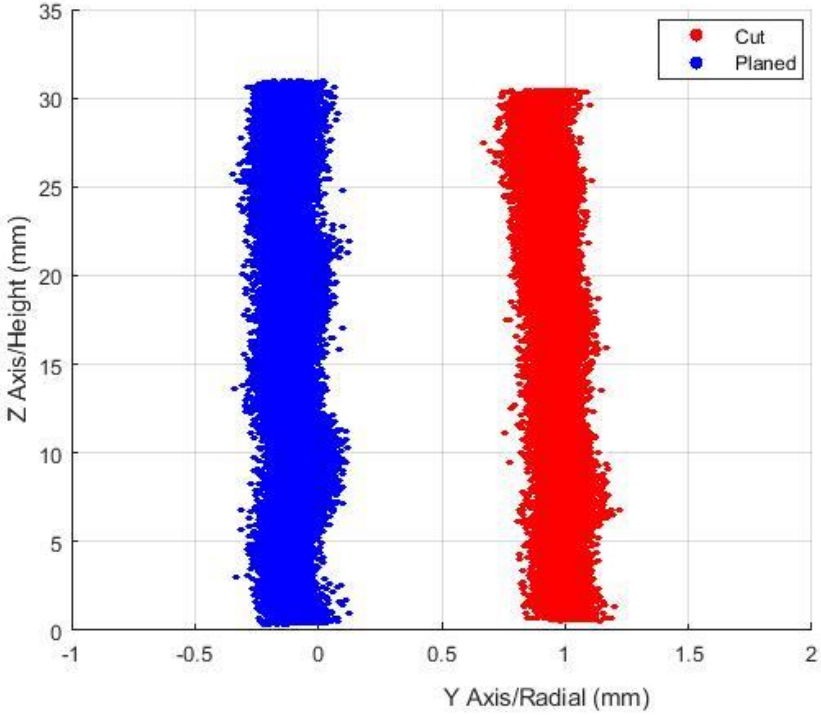

Figure 3.11. End views of the planed and cut surface point clouds of 4 mm plate.

The nominal depth of cut is the radial DOC that is programmed into the path including the desired DOC and path compensation. The measured part error is the difference between the measured machined surface and the desired 1 mm cut surface. Negative values indicate an undercut where less than 1 mm of material was removed and positive values indicate an overcut. Using the measured part error, an improvement is determined as a percentage of the non-compensated experimental measured part errors displayed in Table 3.1. The improvement represents the percentage of the error that has been decreased due to the iterative compensation strategy. The results of the iteratively-compensated cuts are listed in Table 3.3.

Table 3.3: Measured part errors for compensated cuts

Starting Part Thickness (mm)	Nominal Depth of Cut (mm)	Measured Part Error (mm)	Improvement (%)
6	1.16	–0.04	73.25
5	1.20	–0.03	82.47
4	1.28	0.01	94.29
3	1.37	–0.03	88.56

The iterative compensation methodology decreased the part wall thickness error to within 0.05 mm of the nominal thickness for all cases, suggesting that the method is highly effective. The reduction in part wall thickness error ranged from 73.25 to 94.29%. It should be noted that the measured part wall thickness error for the 6 mm and 5 mm thick workpieces were due to an overcut while the measured part error for the 4 mm and 3 mm thick workpieces were due to an undercut. This transition from overcut to undercut indicates an inflection in the effectiveness of the compensation strategy with the inflection

point located at a thickness of 4 mm. Therefore, while the iterative compensation strategy is effective, it is likely there is an effective range for the strategy corresponding to the physical attributes of the part. The cubic dependence of part compliance on the thickness of a plate uses an assumption that the deflections of the plate are small. This assumption may not hold for extremely thin workpiece. However, within the scope of the experiments, the data driven compensation strategy is shown to successfully minimize the wall thickness error.

An intriguing observation is the measured part error is consistently within 0.05 mm when using the data driven iterative compensation strategy. As mentioned previously, the positional accuracy of the robot with real time corrections has been demonstrated to be within 0.08 mm [12], which is double the maximum error observed with path compensation. This increased precision of path control can be attributed to the elimination of factors impacting machining and robot path accuracy inherent in the use of a data driven methodology. The previously mentioned 0.08 mm accuracy is determined through the articulated arm robot's adherence to a given desired path using PID control. In this position tracking there are errors that contribute to the total positional accuracy of the robot including kinematic errors, robot repeatability errors, robot joint compliance, etc. In comparison, the above experiment had a known starting robot pose for consistent joint stiffnesses throughout the milling operation and the path was confined to a short 100 mm path due to the small size of the workpiece. As a result, kinematic errors and joint compliance errors are effectively minimized in the compensated tests, resulting in higher positional accuracy. The remaining factors include robot repeatability, which is 0.08 mm and comparable to the errors observed.

3.6 Summary

A data driven iterative compensation strategy was used to compensate for part deflection during peripheral milling operations of a thin-walled aluminum workpiece. The compensation strategy uses the percentage error of a non-compensated experiment to determine the expected radial depth of cut using a simple geometric series. Non-compensated experiments yielded the baseline machined thin-walled part accuracy obtained with active robot position feedback control. As the part wall thickness decreased, the machined part error increased due to the increased compliance of thin-walled structures. Experimental error in the milled part wall thickness was determined from measurements of the milled surface relative to the initial part surface location. The data driven compensation strategy was found to effectively eliminate between 73 and 94 % of the part wall thickness error depending on the wall thickness (and therefore part compliance). The final part accuracy for wall thickness ranging from 2 to 6 mm was determined to be within 0.05 mm of the desired cut wall thickness. These results have shown that the machined part surface error using the data driven compensation strategy removes significant portions of the error as compared to non-compensated milling operations. In an industry setting, the compensation strategy removes the need for a second finishing cut for thin-walled parts with the use of a single sacrificial cut for data collection. Thus, the data driven iterative compensation strategy has been demonstrated to effectively compensate for the compliance of thin-walled parts.

CHAPTER 4

MODEL-DRIVEN ITERATIVE PATH COMPENSATION STRATEGY FOR PERIPHERAL CUTS

4.1 Introduction

Data driven models can precisely describe complex systems as the physical system supplies the data that is used to build the model. This use of direct inputs and outputs in the creation of the model leads to unexpected phenomena to still be incorporated into the model. However, two clear downsides to the use of data driven models in a machining environment are lack of transparency of the system model and need for time and material intensive data collection. The previously mentioned benefit of data driven models accounting for unexpected phenomena similarly detracts from the quality of the model. These undefined additional factors should be determined through physics-based understanding of the system to fully characterize the factors in the system. Additionally, the data collection process to create high quality data driven models can be time and material intensive especially in the aerospace industry. To replicate the exact conditions of milling on a wing rib structure, multiple wing ribs could be necessary, which can be cost-prohibitive in practice.

For these reasons, a theoretical model is often more desirable than a data driven model if the accuracy of the models is comparable. The objective of this chapter is to create a mechanistic model-based iterative compensation strategy to compensate the robot milling trajectory for part compliance induced part dimensional errors. A model driven compensation approach for the robotic milling of compliant materials must factor the material and shape of the workpiece, machining forces, workpiece fixturing, and

compliance of the workpiece during machining. The new model-based compensation strategy is validated using the same experimental setup described in the previous chapter and the results are compared with the data-driven model-based approach presented earlier.

4.2 Milling Force Model

This section describes the modeling of the milling forces involved in the machining of aluminum. The milling force model used is a static mechanistic force model which relates the milling forces to theoretical chip load as established in previous literature [33]. The forces can be modelled for constant, nominal feed rates when chip dimensions are determined by the feed rate, axial and radial depths of cut, and the cutting tool geometry. The cutting tool is split into discrete disks along the axis of the tool to calculate the cutting force at each point of contact between the helical cutting edges and the workpiece. Then the forces acting on each cutter tooth in each disk are added to determine the total instantaneous forces acting on the cutter at a given cutter rotation angle. This procedure is summarized in pseudocode in Figure 4.1 along with a diagram of the discretized tool below in Figure 4.2. An assumption that is made in this portion of the force analysis is that the workpiece is rigid. This assumption is made to create a naïve rigid force model to demonstrate the use of a force model in tooltip path compensation and is relaxed later to demonstrate the impact of part compliance on cutting forces and path compensation. Another assumption made is that the effects of cutter runout are minimal and do not need to be modelled. This assumption is made as the that the effect of effect of cutter runout is considered small relative to the influence of part compliance.

Inputs

Cutting conditions	$a, c, n, \phi_{st}, \phi_{ex}$
Tool geometry	D, N, β
Cutting constants	$K_{tc}, K_{rc}, K_{te}, K_{re}$
Integration angle	$\Delta\phi$
Integration height	Δa

Outputs

Cutting force history	$F_x(\phi), F_y(\phi), F(\phi)$
Cutting torque and power history	$T_c(\phi), P_c(\phi)$

Variables

$\phi_p = \frac{2\pi}{N}$	Cutter pitch angle
$K = \frac{2\pi}{\Delta\phi}$	Number of angular integration steps
$L = \frac{a}{\Delta a}$	Number of axial integration steps
$i = 1$ to K	Angular integration loop
$\phi(i) = \phi_{st} + i\Delta\phi$	Immersion angle of flute's bottom edge
$F_x(i) = F_y(i) = F_t(i) = 0.0$	Initialize the force integration registers
$k = 1$ to N	Calculate the force contributions of all teeth
$\phi_1 = \phi(i) + (k-1)\phi_p$	Immersion angle for tooth k
$\phi_2 = \phi_1$	Memorize the present immersion
$j = 1$ to L	Integrate along the axial depth of cut
$a(j) = j \cdot \Delta a$	Axial position
$\phi_2 = \phi_1 - \frac{2\tan\beta}{D} a(j)$	Update the immersion angle due helix
if $\phi_{st} \le \phi_2 \le \phi_{ex}$	If the edge is cutting, then
$h = c\sin\phi_2$	Chip thickness at this point
$\Delta F_t = \Delta a(K_{tc}h + K_{te})$	Differential tangential force
$\Delta F_r = \Delta a(K_{rc}h + K_{re})$	Differential radial force
$\Delta F_x = -\Delta F_t\cos\phi_2 - \Delta F_r\sin\phi_2$	Differential feed force
$\Delta F_y = \Delta F_t\sin\phi_2 - \Delta F_r\cos\phi_2$	Differential normal force
$F_x(i) = F_x(i) + \Delta F_x$	Sum the cutting forces
$F_y(i) = F_y(i) + \Delta F_y$	contributed by the all
$F_t(i) = F_t(i) + \Delta F_t$	'active edges
else	
next j	
next k	
Resulting cutting force values at immersion angle $\phi(i)$	
$F(i) = \sqrt{F_x^2(i) + F_y^2(i)}$	Resultant cutting force
$T_c(i) = \frac{D}{2}F_t(i)$	Cutting torque
next i	
Plot $F_x(i), F_y(i), F_i, T_c(i)$ with varying immersion $\phi(i)$	
stop	
end	

Figure 4.1: Visualization of chip formation for one tooth of cut in climb milling [33]

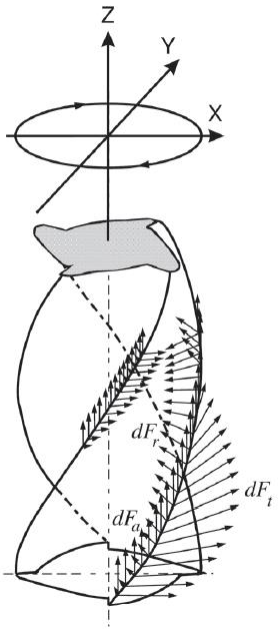

Figure 4.2: Visualization of discretized axial, radial, and tangential forces for cutting tool contact with workpiece [33].

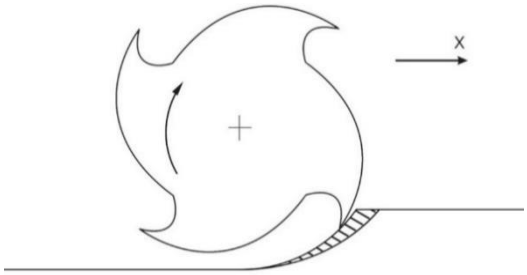

Figure 4.3: Visualization of chip formation for one tooth of cut in climb milling

A visualization of the machining process from a top-down view for the discussed machining conditions are shown in Figure 4.3. During peripheral milling, the X axis represents the feed and any movement of the tool or part in this axis does not impact the cut surface accuracy but rather the feed per tooth, while the Z axis represents the axial DOC which similarly does not impact cut surface accuracy. However, for certain applications, the axial DOC may be a critical dimension and can be compensated for in addition to the

radial DOC. Thus, only the Y axis forces are considered for part deflection calculations. This is similar to the approach used in previous studies where only the Y forces are used for part deflection calculations [33].

The force model must be calibrated for the desired range of cutting conditions by determining the ploughing and cutting coefficients: K_{tc}, K_{rc}, K_{ac}, K_{tr}, K_{re}, and K_{ae}. These cutting force coefficients can be determined through a series of linear slotting cuts where the cutting forces are measured. For this calibration, a 30° helix, 2 flute 19.05mm diameter TiN coated HSS end mill was used to mill a 1.27 mm deep slotting cut on a 25.4 mm thick plate of 6061-T6 aluminum test workpiece. The cut was performed on a milling machine, the Okuma Millac 3-axis CNC, with the forces recorded through a Kistler 9275B Multi Component Dynamometer. Although the tool used differs in diameter from the tool used in experiments, the cutting coefficients are primarily a characteristic of the material of the cutter and the material that is being cut. Physical tool variables such as number of flutes, tool diameter can be adjusted as parameters in the cutting force model. The cutting force model was calibrated for the range of spindle speeds and feed rates shown in Table 4.1.

Table 4.1: Spindle speeds and feed rates used for calibration experiments.

Spindle Speeds (RPM)	Feed Rate (mm/s)			
1000	0.64	1.69	2.96	4.23
2000	1.27	3.39	5.93	8.47
2500	1.59	4.23	7.41	10.58

To convert the recorded experimental force data into the cutting coefficients, the following closed forms equations were used with the average recorded forces, the number of flutes, *N*, and the axial DOC, *a* as shown in Equation 4.1.

$$K_{tc} = \frac{4\bar{F}_{yc}}{N*a} \quad , \quad K_{te} = \frac{\pi\bar{F}_{ye}}{N*a}$$

$$K_{rc} = \frac{-4\bar{F}_{xc}}{N*a} \quad , \quad K_{re} = \frac{-\pi\bar{F}_{xe}}{N*a} \tag{4.1}$$

$$K_{ac} = \frac{\pi\bar{F}_{zc}}{N*a} \quad , \quad K_{ae} = \frac{2\bar{F}_{ze}}{N*a}$$

Using the calibrated mechanistic force model, the cutting forces were modelled during the duration of the cut as shown in Figure 4.3. The cutting conditions simulated are a 1 mm radial DOC, 35 mm axial DOC, 41 mm/min feed rate using a 4 tooth, 30° helix end mill at 1000 rpm. The modelled Y cutting forces are consistent throughout the duration of cut due to the cutting parameters as a tooth engages the workpiece slightly before the prior tooth disengages the workpiece. The cutting forces for an individual tooth engaging the workpiece is shown in Figure 4.4 to demonstrate the individual tooth contributions. The duration of tooth engagement is 114.1° causing a 24.1° overlap between teeth indicated by the cyclical increases and decreases in cutting forces. The average radial cutting force during the duration of cut is 166.79 N with a minimum of 164.51 N and maximum of 174.82 N. The peak forces of 174.82 N occur when two teeth engage the workpiece at a single time as the peak modelled force of a single tooth is 164.73 N shown in Figure 4.4. During the entry and exit of individual teeth, there are two points of tool contact on the workpiece, which must be considered when applying the simulated forces on the FEM model for simulated part deflection calculations.

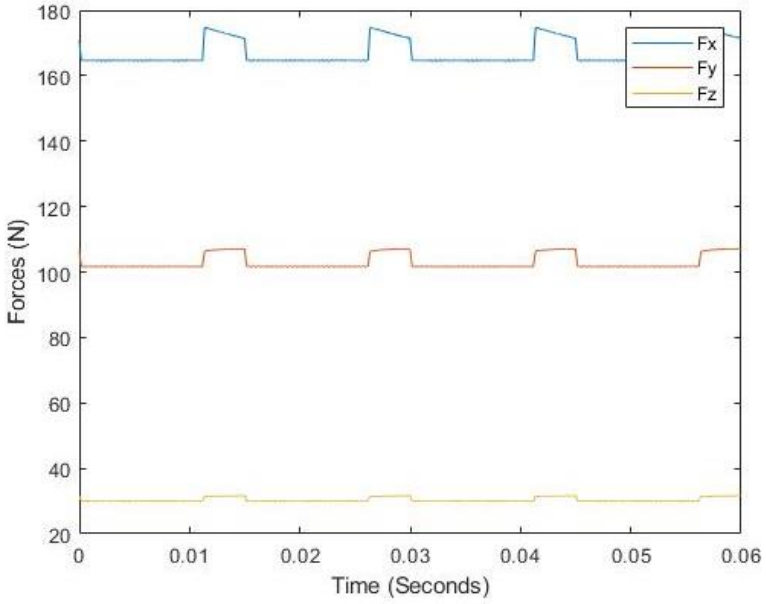

Figure 4.3: Cutting forces over time for one cutting tool revolution (1 mm radial, 35 mm axial, 4 tooth, 30° helix, 1000 rpm, 41 mm/min feed)

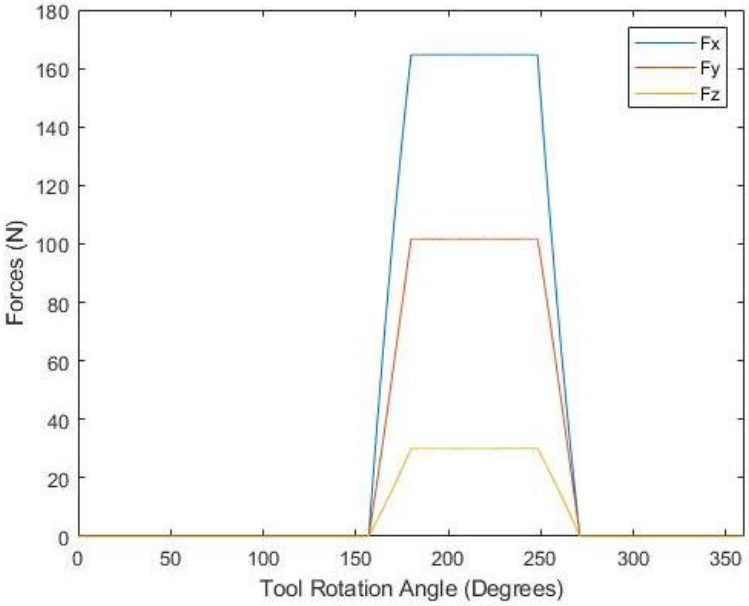

Figure 4.4: Cutting forces versus cutter rotation angle for a single tooth (1 mm radial, 35 mm axial, 4 tooth, 30° helix, 1000 rpm, 41 mm/min feed)

4.3 Part Deflection Model

In order to utilize the simulated milling forces to determine part deflections, a model of the workpiece must also be created. In industry, large scale parts are routinely modelled using Finite Element Modeling (FEM) and Finite Element Analysis (FEA) programs. For the creation of the workpiece compliance model, SolidWorks FEM/FEA software was used. Such modeling software can be utilized to accurately model three-dimensional parts and simulate loading conditions and fixturing constraints. In addition, the modeling software can be used to export the global stiffness matrix to rapidly calculate part deflections outside the FEA software.

For the purposes of workpiece modeling, an idealized, flat aluminum plate of nominal dimensions was used. The aluminum plates used for experiments in this thesis were carefully machined using an OMAX ProtoMAX Abrasive waterjet. Use of the waterjet to machine the 6.35 mm thick aluminum plates created parts with minimal dimensioning errors that would not significantly impact the part deflection calculations. The fixture used for the experiments was a floor mounted vice, which fully constrains all 6 axes of rotation and translation of one edge of the workpiece. The remaining five sides of the workpiece are without fixturing constraints as shown in the CAD model in Figure 4.5. A tetrahedral element size of 0.3 mm was used for a total of 1,837,554 elements as shown in Figure 4.6. This high number of elements ensures that the simulated point load force can accurately simulate part deflection. A convergence study was used to determine the viability of the meshing parameters as the change in simulated deflection for 0.3 mm to 0.35 mm mesh size is less than 0.02% of the total deflection. A lesser number of elements could negatively impact the FEA model as the simulated deflections may not have

converged to a stable value. Separate from the meshing parameters, a grid of points for force application were generated where the simulated machining forces are applied. The points of force application are a grid of nodes spaced at 5 mm increments as used in prior works for modeling where the simulated machining forces are to be applied [33]. It is noted that the top and bottom 5 mm of the workpiece had nodes even spaced at 1.66 mm increments instead of 5 mm as shown in Figure 4.7. This finer discretization at the top 5 mm and bottom 5 mm is necessary as the magnitude of force applied changes rapidly at the bottom and top of the workpiece as the cutter tooth enters and leaves the workpiece, respectively.

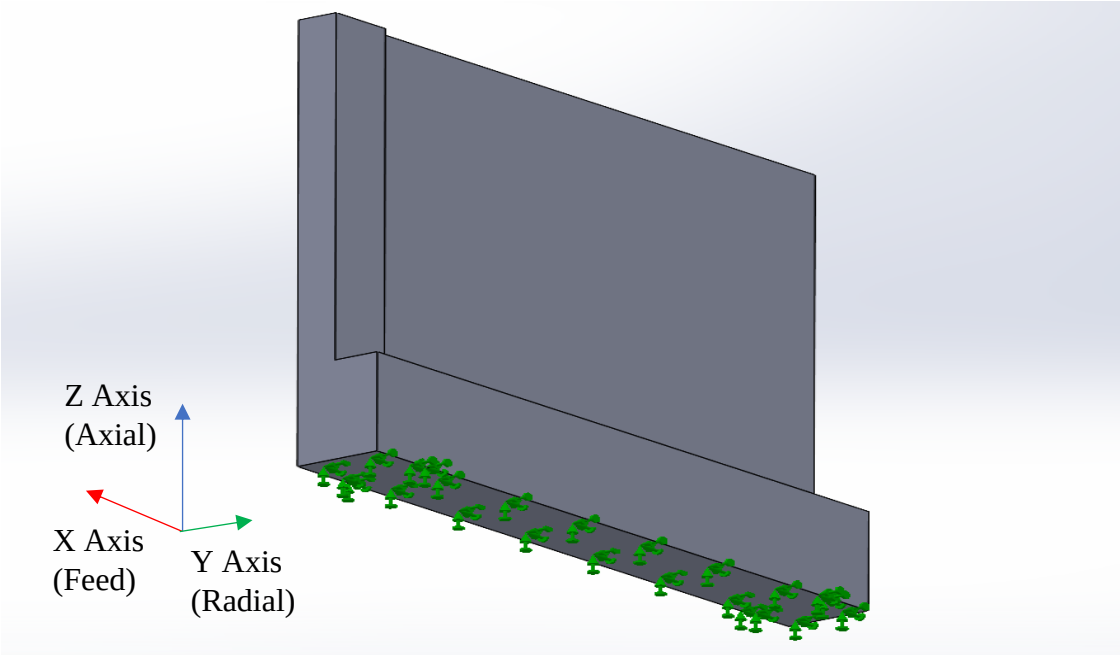

Figure 4.5: CAD model of 3 mm thick part with 6DOF fixturing constraints on bottom surface

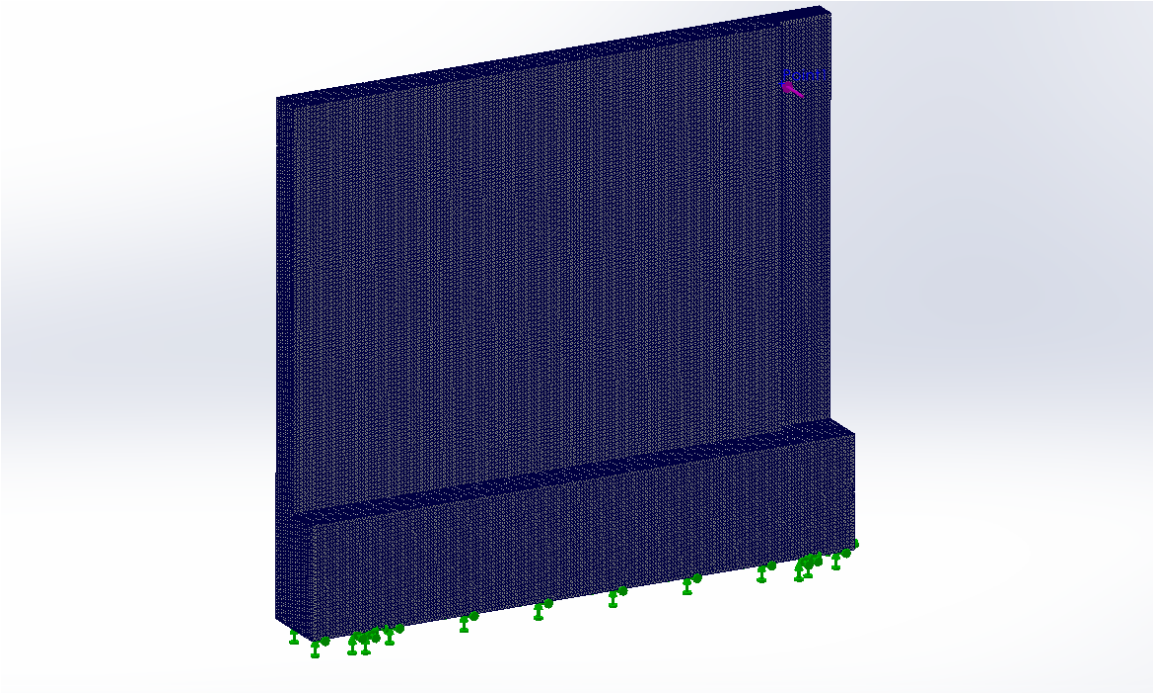

Figure 4.6: FEA model of 3 mm thick part with meshing of 0.3 tetrahedral elements size and 1,800,000 total elements

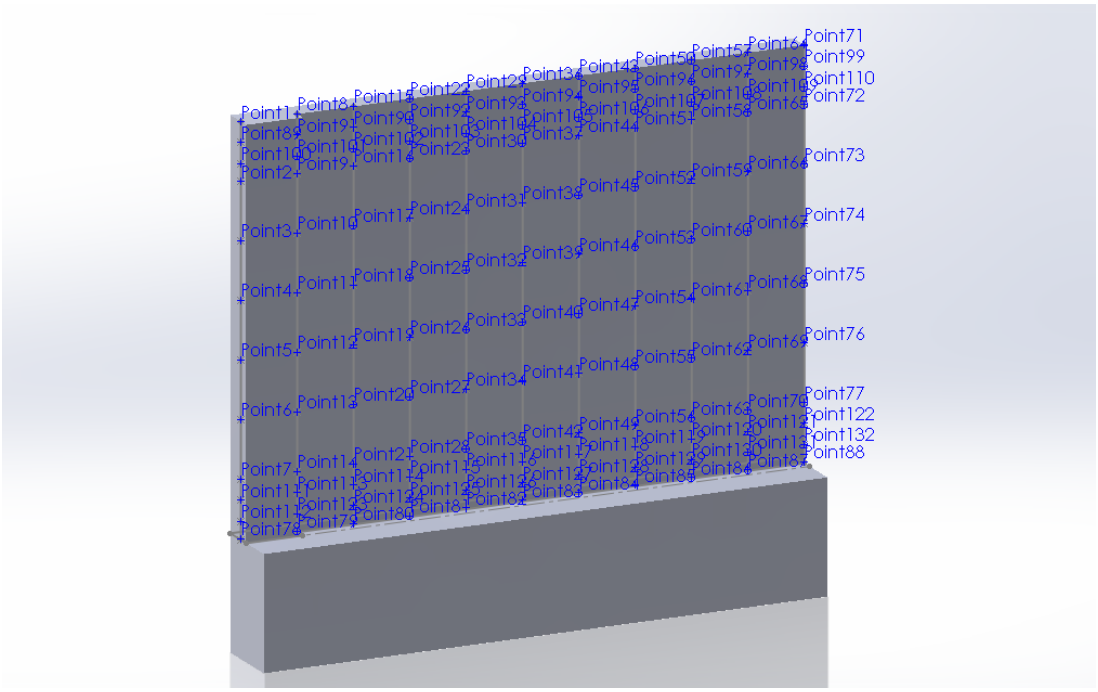

Figure 4.7: CAD model of 3 mm thick part with points of force application in 11x12 grid

During machining experiments, the end mill was programmed to machine 5 mm from the top of the vice which results in an unmachined portion of the workpiece. This is represented in the modelled FEA part as a constant 6.35 mm thick and 5 mm tall base for the part that is fixed at the bottom. Since the nominal radial depth of cut in all experiments was 1 mm, the starting plate thicknesses modelled using FEA ranged from 6, 5, 4, to 3 mm. To model these parts, a variable part geometry model is used as the part changes thickness throughout the cut. For example, the 4 mm thick starting plate is machined down to 3 mm. At the start of the cut, the machining forces are applied to a 4 mm plate. However, as the cut progresses, the plate becomes thinner as material is removed, leaving the final plate just 3 mm thick. Given that the plate is now 25% thinner, the compliance of the part for a constant applied force is significantly greater. This variable plate thickness was modelled using an additional ridge to simulate the uncut and cut regions of the workpiece. In Figures 4.8, 4.9 and 4.10, the start, middle and end of the simulated milling of a 4 mm thick workpiece is modelled where the tool feed direction is from right to left. An assumption made is that the transition of the uncut and cut regions does not significantly impact the model as it relates to stiffness. The transition between these two regions can be modelled as a curve, following the natural curvature of the cutter. However, for simplification and generalization of the CAD model, a distinct immediate increase in plate thickness was used. This allows for the model to be rapidly adjusted for varying depths of cut with minimal additional model changes.

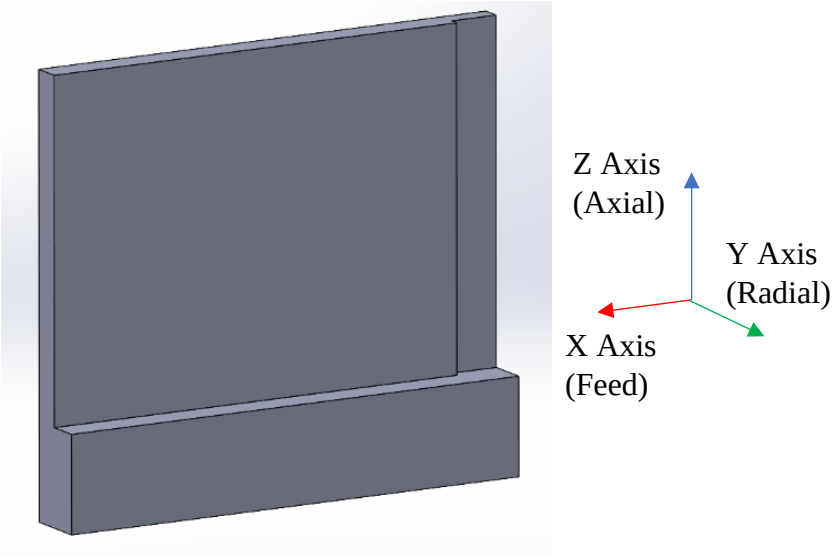

Figure 4.8: CAD model of 3 mm thick workpiece, undergoing 1 mm radial peripheral milling operation (5 mm of cutter engagement in feed direction)

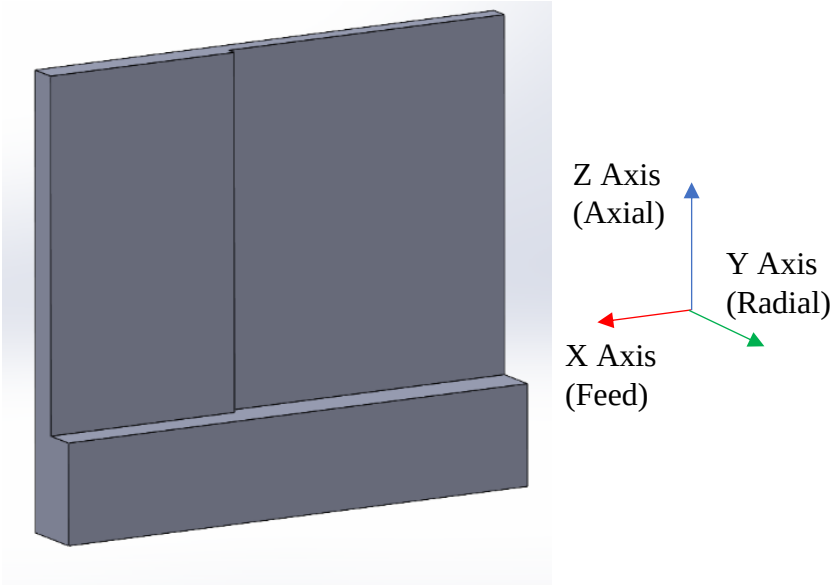

Figure 4.9: CAD model of 3 mm thick workpiece, undergoing 1 mm radial peripheral milling operation (35 mm of cutter engagement in feed direction)

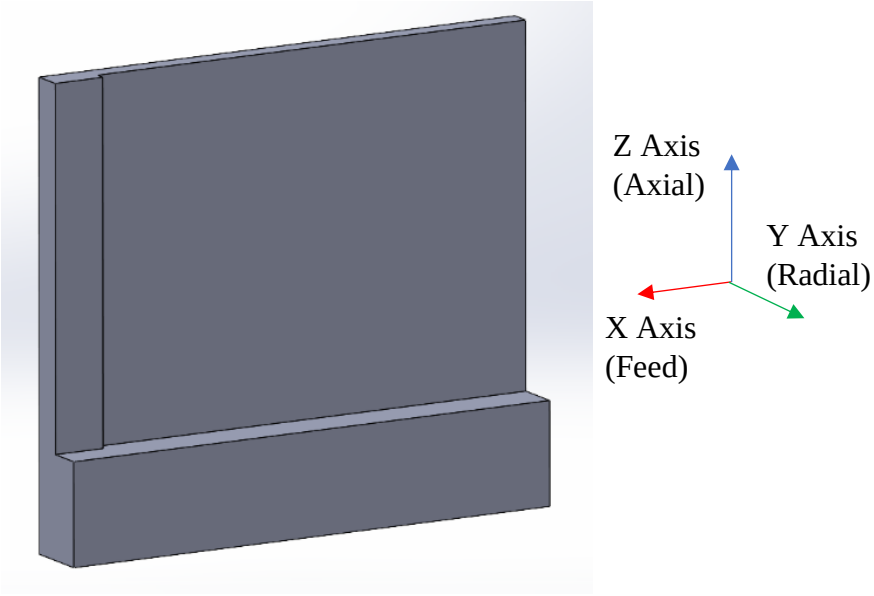

Figure 4.10: CAD model of 3 mm thick workpiece, undergoing 1 mm radial peripheral milling operation (45 mm of cutter engagement in feed direction)

To apply the simulated milling forces to the FEA model, it is critical to make assumptions on how the simulated forces of the tool are being applied to the workpiece. The first assumption is that the simulated forces can be modelled as a point load on the workpiece. This assumption is made based on the low radial DOC (1 mm) relative to the 25.4 mm diameter tool used in the experiments. When a cutter tooth is fully engaged with the workpiece, the contact area follows the edge of the tool along a limited portion depending on the radial DOC and feed per tooth. Through simple geometry, it can be determined that the total contact length along the edge of a tooth is a 10.15 mm arc with 5 mm width and 8.79 mm height as shown in Figure 4.10. This arc is a small region of the whole workpiece, allowing for the assumption that the force is experienced at a point at the center of the contact arc rather than a region of the workpiece. This simplification of the

region of force application into a single point allows for a single point load to be applied to the FEM model rather than a distributed load.

In prior works, the concept of a force center is defined as the point of application of the Y point force necessary to produce the same bending moment in the tool holder as the distributed load on the cutting tool [33]. In addition, the surface generation point is the point of the workpiece that remains after the machining operation is completed. The surface generation point is critical to track as all other points will be removed by the subsequent teeth that engage with the workpiece. The force center can differ from the surface generation point if the cutting tool is compliant or the cutting forces are modelled as a distributed load. Thus, an assumption is made that the cutting tool and robotic arm are significantly more rigid than the compliant workpiece. As the milling force is assumed to be concentrated at the center of the contact arc between the cutter tooth edge and the workpiece, the surface generation point can be approximated to be at the force center as the surface is generated by the cutter at the point of force application.

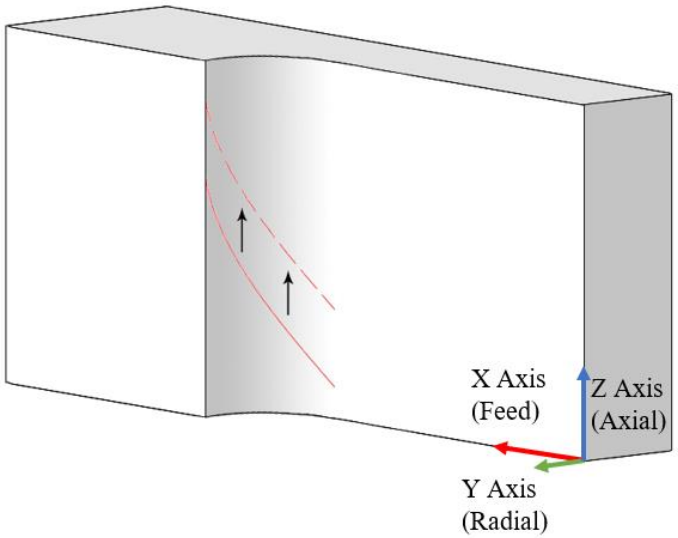

Figure 4.11: Visualization of contact arc (in red) between cutter tooth and workpiece

The simulated milling force is applied at the force center and the deflection determined at that location is the part compliance error at the surface generation point. The peak simulated Y axis force for a single tooth is 164.73 N as modelled with the specific cutting conditions previously described. This force was applied to the nodes in the center 25 mm of the part of the FEA model and the calculated static deflections were recorded. The top and bottom 5 mm did not have this average force applied as the tool teeth are engaging/disengaging at those locations and have less force applied. As previously discussed, the cutting force varies from this constant value when the tooth is starting to engage or disengage the workpiece. To determine the applied forces as the tool enters and leaves the workpiece, the load at the given Z axis location must be determined. The cutting force model simulates the instantaneous cutting forces for a given cutter rotation angle while the helix angle of the tool relates the rotation angle of the tool to the Z axis location of the force center. Thus, the tool entry and exit forces were determined as displayed in Table 4.2.

Table 4.2: Table of simulated Y axis force values used for Z axis locations in FEA

Z axis location on FEA Workpiece (mm)	Simulated Y force (N)
0.00	0
1.67	37.18
3.33	71.66
5.00	103.49
10-25	164.37
30.00	84.52
31.67	54.07
33.33	25.39
35.00	0

Intuitively, the Y axis simulated cutting forces increase as the tool engages in climb milling near the bottom of the part from 0 to the peak of 164.37 N with full tooth engagement occurring at 8.79 mm from the bottom of the workpiece. Conversely, as the tooth disengages the workpiece, the forces decrease. The rate of change of the cutting forces is not the same for engaging and disengaging the workpiece as climb milling was used, causing the tooth entry forces to increase more rapidly than when the tool exits the workpiece. Sample images of the application of force at the force center is shown in Figures 4.12, 4.13, and 4.14.

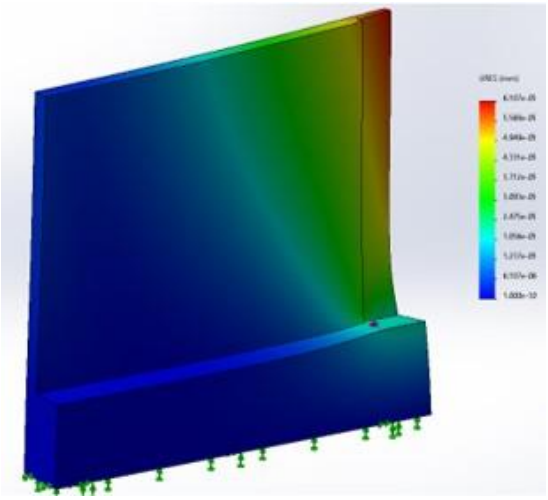

Figure 4.12: FEA of force application at force center 5 mm into cut of 4 mm thick workpiece

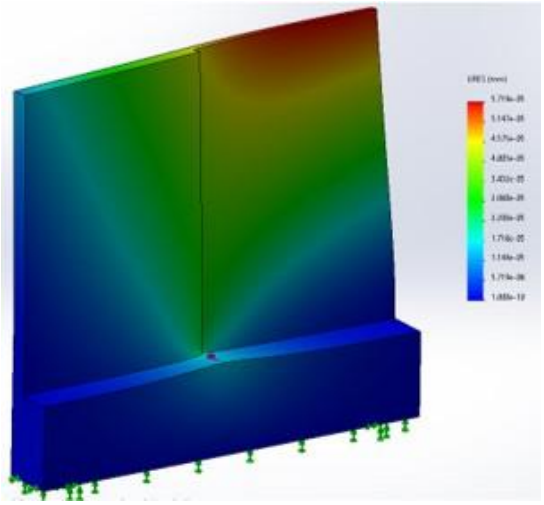

Figure 4.13: FEA application of force at force center 30 mm into cut of 4 mm thick workpiece

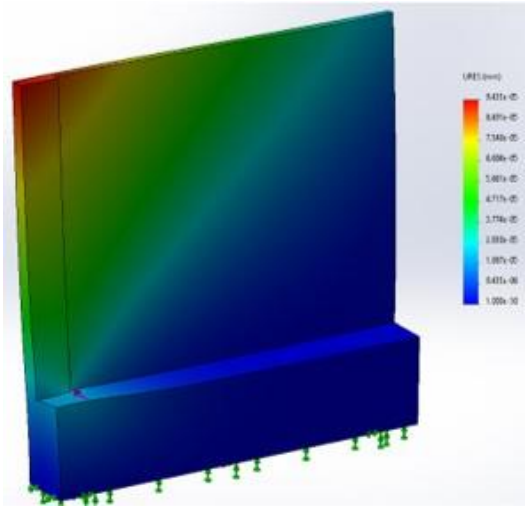

Figure 4.14: FEA application of force at force center 45 mm into cut of 4 mm thick workpiece

4.4 Model Based Path Compensation Strategy

In this section, the previously described iterative compensation strategy is used albeit with the model-based part deflection values. The key downside of the data driven strategy presented earlier is that model calibration experiments must performed to determine part deflection values for the path compensation strategy. Applying simulated

milling forces to a finite element model of the workpiece yields a model-based deflection, thereby eliminating the need for sacrificial model calibration experiments. In the application of the simulated forces to the FEA model, a naïve application of Hooke's law can be used to develop a linear relationship between the machining forces and the deflection of the part. However, this initial naïve model makes two assumptions. The first assumption is that the part will deflect linearly for a given force. Nonlinear behavior can occur for deflection for very thin parts or when deflection of the part is large, thus this assumption may not hold true for very thin workpieces. For beam and plate bending equations, small deflections are a frequent assumption made to allow linear relationships between loads and deflections. The second assumption is that the mechanistic force model will remain constant while the part is deflecting. As discussed earlier, the mechanistic force model simulates milling forces based on deterministic chip formation characteristics assuming a rigid tool and a rigid workpiece. However, in the case of machining compliant parts, this assumption cannot be made as the workpiece is significantly compliant. Thus, the deflection of the workpiece must be used to recalculate the simulated, which leads to new workpiece deflections and new simulated forces until there is an equilibrium is reached between the computed deflection and the simulated machining force. It is important to understand that the data driven model intrinsically accounted for this equilibrium.

4.4.1 Rigid Model Based Compensation

The rigid FEA model-based compensation strategy directly applies the simulated milling forces to the FEA model of the fixtured workpiece at the corresponding points to determine the deflection of the workpiece at each location. The forces listed in Table 4.2 were applied to each point at the corresponding nodes in the finite element model. For each

starting plate thickness of 6, 5, 4, to 3 mm, a total of 132 FEA force simulations were run. The result of these simulations is a grid of modelled part deflections at each node on the surface of the part as shown in Figure 4.15, which shows a heat map of the simulated part deflection for the 4 mm plate thickness case.

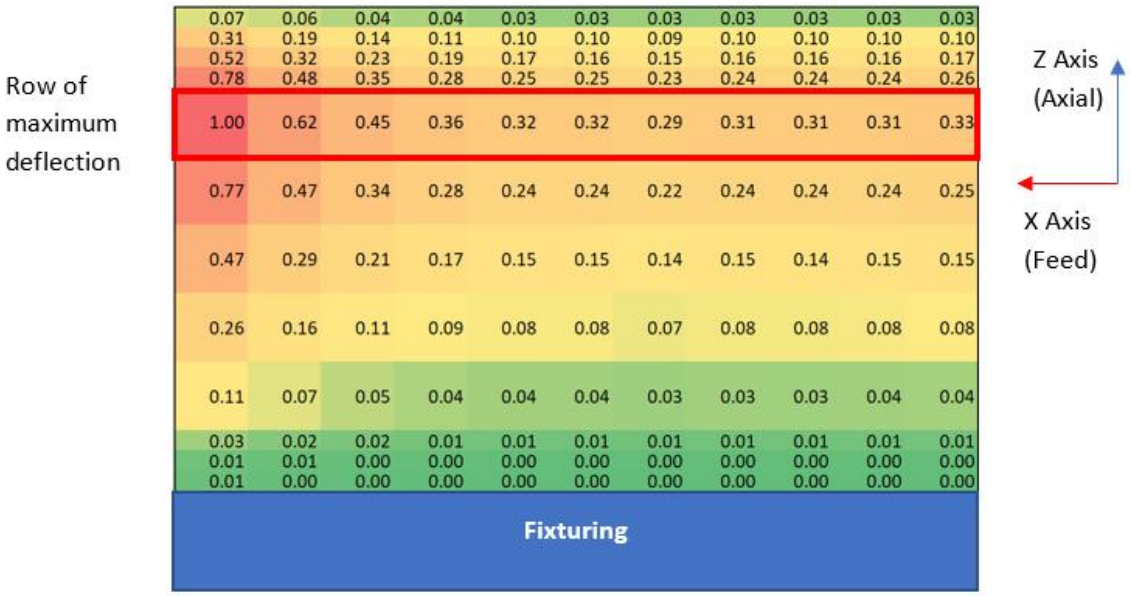

Figure 4.15: Simulated workpiece deflection heatmap (mm) of the 4 mm thick workpiece during simulated machining forces of 1 mm radial DOC.

As displayed in the figure, the modelled part deflects between 0.00 to 1.00 mm depending on the location on the workpiece. The deflection is minimal in the bottom 5 mm of the part, with a maximum deflection of 0.03 mm, and increases as the force is applied further up on the part. This is an expected result as the workpiece acts as a cantilevered plate that is fixed at the bottom with the other three edges free. The fixed edge will not display significant deflection even with significant forces applies due to the higher stiffness of the part in this region. Two interesting aspects of the part deflection heatmap are that there is decreasing deflection near the top of the part and increasing deflection near the end

of the cut on the left. The decreased compliance at the top can be attributed to the decreasing simulated forces as the cutter tooth is exiting the workpiece. This was modelled using decreasing force loads as the force centers neared the top and bottom of the workpiece. The physical significance of this decrease in the milling forces near the top of the part should be seen as the part bending away from cutter as the force center travels up the workpiece but relaxing back into the cutter as the tooth exits and the compliance decreases. The second effect of compliance is due to the decreasing thickness of the plate as the workpiece is being machined. As the simulated magnitude of force does not change throughout the machining path, the resulting part compliance is greatest when the part is thinnest and has the lowest stiffness. These two conditions are met near the top left corner of the part when the plate is thinnest and furthest from fixturing.

To incorporate the modelled compliances into the iterative path compensation strategy, the grid of part deflections must be condensed into a single part deflection error value represented as a percentage of the nominal radial DOC. As the cutter contacts the workpiece along the Z axis, the compensation value must be equal to the maximum deflection for the cutter at a given location, thus the maximum deflection values of each column are used for compensation calculations as highlighted by the red box in Figure 4.15. However, for the iterative path compensation strategy previously discussed, a single error value is used rather than a series of deflection along the length of cut in the feed axis. Thus, the deflection values are averaged along the length of cut to determine a best fit deflection value. The largest values for a given column were used to account for the maximum deflections that could occur for a given instant in the machining operation. An alternate method of calculation is to average the deflection of the entire column, however,

for model simplicity, only the maximum deflections were used. The impact of this decision is further discussed in Section 5.3.

An exception is made for the two left-most points and the deflections at these locations are not considered in the average deflection for use in path compensation. This exception is due to the fact that the Y-axis machining forces are decreased at the end of cut. The force model utilizes the ideal undeformed chip geometry to determine the cutting forces and relies on consistent chip thickness and cutting conditions. However, as the entire tool leaves the workpiece, the Y component of the machining force rapidly decreases as shown in Figure 4.16. Thus, the left two simulated deflections are not used as they correspond to the point at which the cutter is disengaging the workpiece and the mechanistic force model no longer accurately predicts the cutting force components.

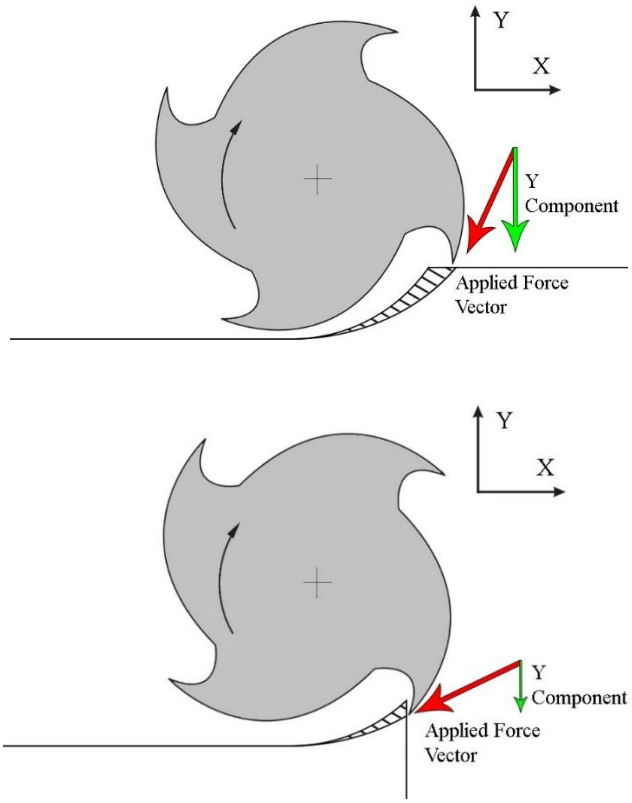

Figure 4.16: Down milling forces generated before and after workpiece edge is reached.

The workpiece compliance modeling was completed for all four experimental plate thicknesses ranging from 6 to 3 mm and the workpiece compliances were averaged. As the experimental setup uses repeatable fixtures and planing cuts for a consistent starting workpiece surface, part compliance induced error is considered to be the major source of the machined part error. Using the iterative compensation strategy presented earlier, the averaged deflections determined from the FEA were input to the geometric series as errors and the corresponding compensated radial DOC values were determined for all experimental plate thicknesses. The plate thickness, modelled part deflection, and the resulting compensated nominal DOC are given in Table 4.3. Although the rigid FEA model based compensated radial DOC values are similar to the values determined using the data driven approach presented earlier for plate thicknesses from 6 to 4 mm, the rigid model deviates significantly for a 3 mm thick plate. The naïve rigid model outputs an unrealistic value (4.341 mm) for the compensated radial DOC for a 3 mm thick workpiece, far surpassing the entire thickness of the workpiece itself, suggesting the negative impact of the assumption of simulated part deflection not impacting the simulated deflection forces.

Table 4.3: Rigid model-based compensation radial deflection and DOC

Plate Thickness (mm)	Modelled Part Average Deflection (mm)	Compliance Error Fraction (%)	Compensated DOC (mm)
6	0.12	12	1.136
5	0.17	17	1.205
4	0.33	33	1.483
3	0.77	77	4.341

4.4.2 Compliant Force Model Based Compensation

The naïve rigid force model assumed that the instantaneous forces causing part deflections were not affected by the deflections. This assumption is flawed as the modelled part deflections reported in Table 4.3 ranged from 0.12 mm to 0.77 mm. This deflection directly impacts the mechanistic force model as the chip thickness is decreased by the part deflection. For the 3 mm thick plate, the force model assumes a 1 mm nominal radial depth of cut, although the deflection for the given force value was determined to be 0.77 mm, which suggests an actual radial depth of cut of 0.23 mm and an updated radial force of 69.99 N. However, this final force cannot be directly used for the calculation of the compliance in the FEA model. As the simulated force is impacted by the simulated deflection, the deflection must be determined for the updated simulated force, demonstrating the need for an iterative method to determine an equilibrium where the simulated force and simulated workpiece deflection both correspond to each other. This iterative process can be seen in Equation 4.2.

$$\delta_y^i = \frac{F_y\left(d_r^{nom,i}\right)}{k}$$

$$d_r^{act,i} = d_r^{nom,i} - \delta_y^i \tag{4.2}$$

$$d_r^{nom,i+1} = d_r^{act,i}$$

First the nominal radial DOC, $d_r^{nom,i}$, is set as the desired radial DOC. The nominal radial DOC is used in the force model to determine the Y forces, which are applied to the FEA model yielding workpiece deflections, δ_y^i. The actual radial DOC, $d_r^{act,i}$, is determined by subtracting the simulated deflection from the nominal radial DOC. Finally,

the actual radial DOC is then input back into the simulated force model as the updated nominal radial DOC, $d_r^{nom,i+1}$. Through this method, the simulated Y cutting forces were updated for each given part thickness. The method must be repeated for each workpiece thickness as the compliance characteristics change dramatically as the part gets thinner. Both rigid and compliant model based cutting forces as well as their corresponding simulated compliance error fractions are displayed in Table 4.4. Compliance error fractions are calculated by dividing the simulated average part deflection by the nominal radial DOC.

Table 4.4: Rigid and compliant force model-based part compliance error fractions.

Plate Thickness (mm)	Peak Y Force - Rigid Force Model (N)	Rigid Force Model Based Compliance Error Fraction (%)	Peak Y Force – Compliant Force Model (N)	Compliant Force Model Based Part Compliance Error Fraction (%)
6	164.73	11.7	155.46	11.1
5	164.73	16.8	152.08	15.6
4	164.73	32.8	136.50	27.2
3	164.73	85.3	77.36	40.1

Table 4.5: Comparison of compensated radial DOC values for data driven model, rigid and compliant force model based methods.

Plate Thickness (mm)	Compensated Radial DOC - Data Driven Model (mm)	Compensated Radial DOC – Rigid Force Model (mm)	Compensated Radial DOC – Compliant Force Model (mm)
6	1.16	1.136	1.124
5	1.20	1.205	1.176
4	1.28	1.483	1.370
3	1.37	4.341	1.669

The compensated radial DOC values for the data-driven model, the rigid force model based FEA, and the compliant force model based FEA are compiled in Table 4.5. The three models demonstrate consistent trends for plate thicknesses ranging from 6 to 4 mm, with one significant outlier in the rigid force model based FEA case for the 3 mm thick workpiece. The compliant force model based FEA significantly improves upon the naïve rigid force model as the compensated radial DOC is no longer larger than the thickness of the workpiece and is instead of similar magnitude as the value derived from the data driven model. However, there are still additional improvements that can be made in the compliant force model based FEA approach as the compensated radial DOC values are significantly larger than the compensated radial depths of cut predicted by the data driven model. In addition, the compliant force model based FEA approach predicted radial depths of cut seem to increase faster as the plate thickness decreases than the compensated radial depths of cut predicted by the data driven model. The compliant force model based

FEA approach follows the simulation of a cantilevered plate, which has a cubic relationship to its thickness while the data driven model does not follow such an aggressive correlation.

4.5 Machined Part Surface Angle Error Compensation

In the development of the model driven compensation strategies, a series of FE models for determining the part deflections during milling were generated. As previously mentioned, it is clear that there is significant part deflection near the top of the workpiece while there is minimal deflection near the supporting fixture. Model based path compensation is a useful tool for offline tool path correction, despite nominally precise robotic arm end effector control. The main error to be corrected is the error in the radial depth of cut (and hence part dimension) due to compliance of the part, which was demonstrated by the data driven model. However, part compliance not only creates a tool path offset that must be corrected, but also a surface angle error of the machined surface with respect to the XZ plane. This is due to the workpiece's variable stiffness along the Z axis during machining. However, upon completion of the machined path, the workpiece returns to its unloaded state due to the lack of machining forces, which results in the angle part surface error as shown in Figure 4.17. Note that the stiffness of the workpiece is significantly lower than the tool and the robotic arm. This causes the rigid tool to retain its nominal orientation, while the workpiece deflects away from it during machining, resulting in the surface angle error.

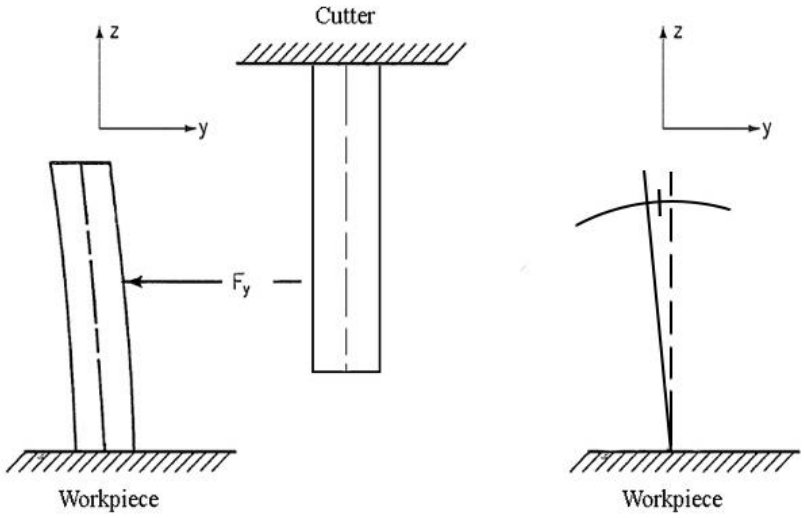

Figure 4.17: Workpiece deflection under cutting conditions creating angled surface

This machined surface angle error effect was consistently noticed in the finite element model-based part deflection analyses and suggests that the additional effect of part compliance can be compensated offline. The 6DOF end effector is programmed to orient the axis of the tool to be parallel to the Z axis of the part frame within 0.01° tolerance. The available degrees of freedom of the robot end effector can be used to correct for the angle error if the error can be estimated from the model. Using the part compliance grid generated for the compliant force model based FEA approach, the row averaged part deflections were used to create a least-squares estimate of the angle error in the YZ plane as shown in Figure 4.18. Note that the least squares estimate of the angle error is only a rough approximation of the actual part surface form but, as will be shown subsequently, is adequate for compensating for illustrating the model-based part surface angle error compensation strategy.

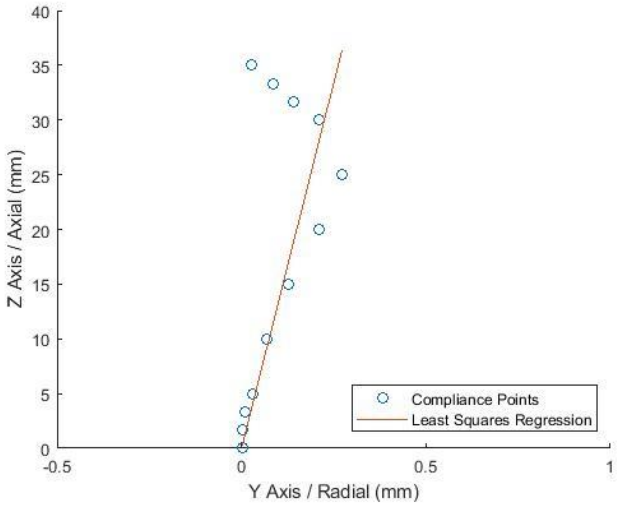

Figure 4.18: Least squares regression of row averaged part deflections taken from the FEA model of a 4 mm thick part.

The angle between the regression line and the Z axis can be calculated to determine the magnitude of part surface angle error expected for each part thickness. The origin was set as the X and Y intercept to aid the regression as there should be no compliance at the origin due to the vise fixture. For these angles, the iterative compensation methodology presented earlier can be applied by defining the error fraction to be ratio between the surface angle and the maximum 90° of potential angling. However, due to the small error fraction, the angles do not change significantly from the regression derived surface angles. The slopes and angles with respect to the Z axis of these regressions for the different plate thicknesses were determined and are given in Table 4.6. The small angles (<1°) are expected as necessary compensation is minimal. For the largest angle error effect on a 3 mm thick part, the iterative compensation methodology increases the tool orientation angle by just over 0.01°, which is of the same order as the repeatability of the laser tracker and T-Mac system.

Table 4.6: Model based estimation of angle error and iteratively compensated angles

Plate Thickness (mm)	Slope (mm/mm)	Equivalent Angle (°)	Angular Compensation (°)
6	324.88	0.187	0.187
5	231.16	0.287	0.289
4	133.56	0.429	0.431
3	89.93	0.962	0.972

This application of the iterative path compensation strategy demonstrates the adaptability of the simple yet effective methodology. The iterative methodology can be rapidly adapted and utilized for use in application for linear translational error compensation or angular error compensation. The effectiveness of the strategy can be difficult to detect when employed for angular path compensation due to the minute differences between the initial input and the iteratively determined angles.

4.6 Experimental Validation

For testing the rigid and compliant force based FEA model-based compensation strategies, experiments similar to those described in Chapter 3 were utilized. The tests are designed to measure the error in the machined part, which is measured using the Leica T-Scan. Machined part accuracy results of the model-based compensation strategy are compared to the results of the un-compensated and data driven compensation methods to determine efficacy and utility of the proposed compensation strategies. Rigid force model based part compliance error compensation uses the iterative compensation methodology with the compliance error fraction determined from the FEA models as input. It should be

noted that the 3 mm thick part was excluded from experimental validation due to the compensated radial depth of cut exceeding the thickness of the part itself. The control variable is the cut part wall thickness for the 6, 5, and 4 mm thick 6061-T6 aluminum plates milled with a 35 mm axial DOC, 1 mm radial DOC, and a 50 mm length of cut as was previously discussed. Similar to the experimental cutting conditions in Chapter 3, the cutting conditions used were 82 mm/min feed rate, 1000 rpm spindle speed, 25.4 mm diameter TiN coated, 4 flute, 30° helix square end mill. After all rigid force model based compensated radial depth of cut experiments were performed, all compliant force model based compensated radial depth of cut experiments were performed. Lastly, the compliant force model-based compensation strategy experiments were performed a second time, with incorporation of the part surface angle error compensation method discussed above. These experiments are compared with the baseline uncompensated experiment results to validate the model based iterative path compensation strategy for both translational and angular part error compensation.

4.7 Results and Discussion

For experimentally validating the rigid and compliant force model-based part error compensation strategies, the robot tool path is offset based on the predicted compensated radial depth of cut for the plate thickness being used. The error values were calculated as the distance between the machined surface measured by a T-Scan and the desired machined surface. The results of the two model-based compensation strategies are shown in Table 4.7 along with the results for the data driven compensation for comparison. The machined part surface data was collected using the Leica T-Scan as a point cloud. A mean plane was fit to the point cloud and the part thickness error (or radial depth of cut error) was

determined as the difference between the mean planes of the machined and the initially planed surfaces. The performance improvement realized from the model-based error compensation strategies is displayed in Table 4.8 as a percentage improvement over the baseline uncompensated error and is computed as in Equation 4.3.

Table 4.7: Results for Data Driven-, Rigid Model-, Compliant Model- based strategies with errors of distance between measured and desired machined surfaces

Part Thickness (mm)	Data Driven Model Based Part Error Compensation (mm)		Rigid Force Model Based Part Compensation (mm)		Compliant Force Model Based Part Error Compensation (mm)	
6	-0.04	± 0.031	-0.02	± 0.033	-0.05	± 0.022
5	-0.03	± 0.045	-0.03	± 0.054	-0.08	± 0.031
4	-0.01	± 0.072	+0.05	± 0.075	+0.03	± 0.067
3	-0.03	± 0.134	N/A	N/A	+0.10	± 0.112

Table 4.8: Percent improvement for Data Driven-, Rigid Model-, Compliant Model- based on experimental results as percentage improvement over non-compensated error

Part Thickness (mm)	Data Driven Model Based Part Error Compensation (%)	Rigid Force Model Based Part Error Compensation (%)	Compliant Force Model Based Part Error Compensation (%)
6	73.25	86.47	66.75
5	82.47	82.45	52.94
4	94.29	77.27	86.82
3	88.56		62.97

$$\% \, Improvement = \left| \frac{d_r^{Non-Comp} - d_r^{Experiment}}{d_r^{Non-Comp}} \right| \quad (4.3)$$

The part errors reported in Table 4.7 were calculated by subtracting the actual radial DOC, determined from the planed and machined part surface measurements, from the nominal radial DOC resulting in overcuts (positive values) and undercuts (negative values). Improvement is defined in Equation 4.3 where $d_r^{Non-Comp}$ is the uncompensated nominal radial DOC and $d_r^{Experiment}$ is the experimentally measured radial DOC.

It is clear from Table 4.8 that the data driven model out performed both the rigid model and compliant force model based compensation methods. This is to be expected since data driven models account for all factors impacting part error, which cannot always be modelled. Some possible sources of error stem from the assumptions made during the model development. Cutter runout was not considered, however for the low feed per tooth used in the experiments, cutter runout can result in underestimation of peak forces, impacting deflection calculations. The machining forces were also assumed to be point loads rather than a distributed load over the entire tool's contact area with the workpiece. A third potential source is the simplification of the CAD model transition between the machined and planed surface of a discrete decrease in plate thickness rather than a curved section which can impact FEA results. Over the four validation experiments, the data-driven model achieved an average improvement of 85.0%. The potential impact of the iterative compensation strategy is significant for the articulated robotic arm machining application considered here as the model-based offline compensation methodology is predictive and can be easily implemented.

Following the data driven model performance, the rigid force model based part compliance error compensation methodology yielded an average part error improvement of 82.1%. This is a dramatic decrease in part dimensional error that is within a few percent of the data driven model without the need for baseline experimental cuts or potentially costly sacrificial materials. Although the rigid model performed well, it is important to note that the percentage improvement did not take into account the 3 mm thick plate experiment, which would have overcut the part by up to 3 mm. This is a significant consideration that must be further inspected as it could suggest that the rigid model is an accurate machining model but for a limited range of applications. For application to thin walled compliant structures, the model does lose some relevance.

The rigid force model assumption was relaxed in the compliance force model based part error compensation strategy. However, based on the experimental results, the compliant force model based error compensation strategy yielded an average improvement of 67.2% with a low of 52.9% improvement during machining of a 4 mm thick workpiece. These low improvements, compared to the data driven and rigid force model strategies, suggests that there are additional factors that were not considered in the creation of the compliant model. These additional factors could potentially be modelled and incorporated to the compliant force model-based part error compensation strategy to yield a fully theoretical and highly effective compensation strategy model. Although the compliant force model based part error compensation strategy did not perform as well as the other models, it is important to understand the clear advantages that the compliant model has over the other two modeling methods. The compliant force model based compensation strategy is theoretical and the most significant components of the model are explicitly

defined as compared to a data driven model where the error sources are not obvious. In addition, as a theoretical approach, time and material consuming data collection can be bypassed completely allowing for faster model development and changes to validation experiments performed to verify the model predicted improvements. With respect to the rigid force model, the compliant force model based compensation strategy is still a better choice as refinements of the assumptions, model components, and system variables are sure to bring the theoretical model closer to the experimental results.

The compliant force model was also used to demonstrate the use of the iterative compensation strategy to remove the part surface angle error that occurs due to the compliance of the part during machining. Due to the significantly higher compliance of the workpiece compared to the end mill, the workpiece retains a majority of the angle that it deflected through during machining as it returns to its unloaded state. Figures 4.19 and 4.20 show the machined part surfaces obtained using no compensation for angle error and using the angle error compensation approach presented earlier for a 4 mm thick workpiece.

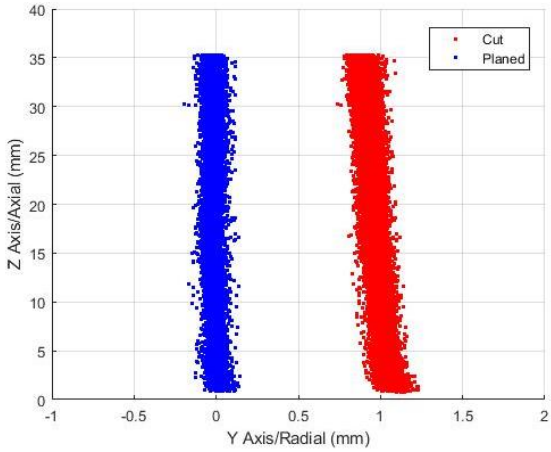

Figure 4.19: Machined surface obtained for a 4 mm thick part using compliant force model based part error compensation strategy without angle error compensation.

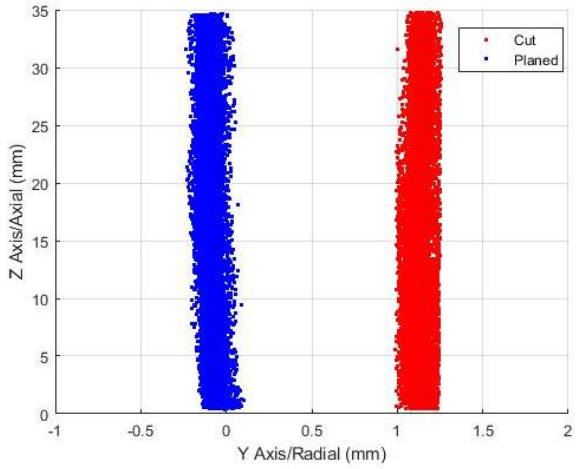

Figure 4.20: Machined surface obtained for a 4 mm thick part using compliant force model based part error compensation including angle error compensation.

As seen in Figure 4.19, the machined surface is noticeably tilted when the angle error compensation is not included. The part surface was measured to be angled by 0.365°, which is close to the simulated value of 0.429°listed in Table 4.6. Compensating for the angle iteratively corrected most of the angle error. Near the top of the angle error compensated machined surface, the surface appears to be somewhat overcompensated. This may be similar to the overcompensation that occurred for thin workpieces when the compliant force model was used. It could also be attributed to the use of a least squares best fit when determining the angle for compensation. It is clear from Figure 4.17 that the best fit line strays from the simulated compliance surface near the top of the part, which could cause this over correction.

4.8 Summary

In this chapter, both rigid and compliant force based theoretical models were explored for use in the iterative path compensation strategy established in Chapter 3. The model-based compensation strategy presented in this chapter proposes a novel combination of previously established mechanistic force models and widely used FEA software to bypass the need for the experiments needed by data driven models. Although both theoretical models proved to be effective for use with the iterative path compensation strategy, the rigid model performed better despite having limitations on applicable workpiece geometries. Through continued understanding of the theoretical models, the compliant force model has the potential to be a generalizable and more robust modeling solution for use in the robotic milling path error compensation strategy with part error improvements ranging from 53% to 86%. The results of this chapter demonstrate the practical applicability of in the model-based part error compensation strategy for robotic milling of compliant parts.

CHAPTER 5

CONCLUSIONS AND RECOMMENDATIONS

This chapter summarizes the main conclusions drawn from this thesis and the original contributions made with notes on future work to expand on the efforts presented.

5.1 Iterative Path Compensation Strategy for Peripheral Milling

- A data driven modeling approach was developed to determine the deflection of a part during machining as a function of the part dimensions.
- The results showed that the iterative data driven model was effective in eliminating a significant portion of the part compliance induced error. The largest and smallest percent reduction in machined part surface errors were 94.29% and 73.25%, respectively.

5.2 Rigid and Compliant Force Models for Path Compensation

- A rigid force model for prediction of part deflection was developed using a mechanistic force model and an FEM model of the workpiece. The main assumption of this model is that the FEA modelled part deflection due to simulated machining forces does not impact the machining forces. The rigid force model was found to overcompensate the part compliance error for the 3 mm thick 6061-T6 aluminum part due to the assumption of a rigid workpiece in the force model.
- A compliant force model, which iteratively adjusts the milling forces to account for part deflection, thereby more closely simulating the actual physical interaction

between the tool and the workpiece, was developed. The same mechanistic force model and FEM methodology were used to develop the compliant force model.

- The output deflections of the rigid and compliant force models were used as inputs to the iterative compensation strategy. The rigid force model yielded a maximum and minimum percent improvement in machined part surface errors of 86.47% and 77.27%, respectively while the compliant force model yielded maximum and minimum part surface error improvements of 86.82% and 52.94%, respectively.
- An extension of the compliant force model was developed to account for the angle error in the part surface due to larger part deflection away from the fixtured edge. The degree of angle error obtained through simulation was 0.429° and was reduced to 0.085° after compensation, yielding an improvement of 80.2%.

5.3 Original Contributions

In this thesis, an iterative offline path compensation methodology based on data-driven and model-based approaches to compensate for part compliance induced part surface errors during robotic milling was presented. While the individual components of the model have been investigated in prior works and the compensation strategy of simply cutting deeper to account for deflection is intuitive, the work presented combines the established models to develop a practically useful part error compensation method for robotic milling applications. Offline path compensation has been used to as an effective strategy for desired tool path control based on robot deflection. The iterative methodology is distinct in the compensation for part deflection through the use of a geometric series to efficiently reduce machined part surface error based on an expected deflection as a percentage of the nominal radial DOC. The incorporation of both the mechanistic force

model and finite element analysis into the path compensation strategy represents a novel use of such models to theoretically predict and compensate for part compliance induced errors during the robotic milling of thin-walled parts. It should also be noted that the simplicity of the iterative compensation strategy allows for applications beyond a static translational path compensation as demonstrated through the part surface angle error compensation method. In addition, such a methodology can also be implemented on traditional CNC machines during machining of thin walled structures.

5.3 Future Work and Recommendations

The iterative path compensation strategy established in this thesis can apply to both robotic and traditional machining of thin-walled structures. In addition, the development of a data driven model and rigid and compliant force-based part error compensation models allows for flexibility of desired model selection based on situational requirements. Therefore, the methods presented in this thesis can be applied to a wide variety of applications. A clear next step is to further refine the compliant force model as the final efficacy of the compliant model was inferior to the rigid force model based compensation strategy. This reduction in model performance can be attributed to additional factors in the machining system that have not been modelled and warrants additional research.

A key aspect of the iterative compensation methodology is also that the compensation can be performed completely offline through model-based predictions. Offline compensation is beneficial as it eliminates the need for costly, high precision laser trackers for active feedback methods and the need for sacrificial experimental data. The experimental setup utilized incorporated a laser tracker to ensure high tooltip 6DOF accuracy, which diminishes the benefits of the offline model. To expand upon the work

presented here, the iterative compensation strategy can incorporate tooltip error through modeling of the articulated robotic arm and tooltip deflection in addition to workpiece deflection. It was assumed that tool deflection was negligible in comparison to the deflection of a thin-walled structure. However, this assumption can be relaxed through additional error modeling. Finally, inherent kinematic errors of the robot can be reduced through use of a local calibration within a small machining volume to completely eliminate the need for a laser tracker. Although the functional workpiece volume would be decreased, additional modeling could improve the robustness of the compliant force model-based compensation strategy and decrease the cost of entry for final part surface error compensation in articulated robotic arm machining.

A final important consideration for future work is the implementation of an improved error model for utilization of the mean radial DOC error in both the data driven and model driven approaches. During the analysis presented, the measured surface of the non-compensated experiments was determined as the plane yielding the lowest RMS error from the measured cloud of points. The RMS determined was close to the expected error from the usage of the T-Scan and laser tracker, validating the results of the plane. However, the measured plane was fitted to the nominal plane which results in information about the measured data points to be lost, such as the angling effect described in Chapter 4. In addition, the error was averaged across the entire length of cut causing any deviations in error compensation along the cut length or axial depth of cut to be lost, further decreasing the spatial dependence of the compliance error fraction. Although this method of averaging and plane fitting yields a single error fraction for use in the iterative compensation strategy, an improved method could utilize a spatially resolved error metric which adjusts the

compliance error along the length of cut. The resulting compensation would no longer be a static path compensation offset value, but a path-dependent varying compensation. In addition, the model-driven approach utilized the maximum errors determined from the FEA which can result in over-compensation. Although the model results indicated an under-compensation, an improved model could be developed to account for the average or RMS compliance as an improved quantification of the error.

Implementation of these recommendations in future work could further increase the applicability of the iterative compensation methodology as well as the reliability of the model-based approach. Such improvements in the machining model and compensation strategy will allow for increased industrial applicability of the proposed methods.

References

[1] Cvitanic, Toni, et al. “Pose Optimization in Robotic Machining Using Static and Dynamic Stiffness Models.” *Robotics and Computer-Integrated Manufacturing*, vol. 66, 2020, p. 101992., https://doi.org/10.1016/j.rcim.2020.101992.

[2] Kencoa Aerospace. “Monolithic Machined Wing Rib.” *Kencoa Aerospace LLC | Precision Machining | Sheetmetal Fabrication | Complex Assembly | Engineering | AS9100 | ITAR | SBA Hubzone | Minority Council Certified*, 23 July 2017, https://kencoaaerospace.com/photogallery/monolithic-machined-wing-rib/.

[3] Cen, Lejun, and Shreyes N. Melkote. “Effect of Robot Dynamics on the Machining Forces in Robotic Milling.” *Procedia Manufacturing*, vol. 10, 2017, pp. 486–496., https://doi.org/10.1016/j.promfg.2017.07.034.

[4] Stejskal, Tomáš, et al. “Measurement of Static Stiffness after Motion on a Three-Axis CNC Milling Table.” *Applied Sciences*, vol. 8, no. 1, 2017, p. 15., https://doi.org/10.3390/app8010015.

[5] Cvitanic, Toni, and Shreyes N. Melkote. “A New Method for Closed-Loop Stability Prediction in Industrial Robots.” *Robotics and Computer-Integrated Manufacturing*, vol. 73, 2022, p. 102218., https://doi.org/10.1016/j.rcim.2021.102218.

[6] Del Sol, Irene, et al. “Thin-Wall Machining of Light Alloys: A Review of Models and Industrial Approaches.” *Materials*, vol. 12, no. 12, 2019, p. 2012., https://doi.org/10.3390/ma12122012.

[7] Zhang, Zhijie, et al. “Intelligent Fixture System for CNC Milling Machining of Thin-Walled Structure.” *Proceedings of 2016 International Conference on Modeling, Simulation and Optimization Technologies and Applications (MSOTA2016)*, 2016, https://doi.org/10.2991/msota-16.2016.97.

[8] Bolar, Gururaj, et al. “Measurement and Analysis of Cutting Force and Product Surface Quality during End-Milling of Thin-Wall Components.” *Measurement*, vol. 121, 2018, pp. 190–204., https://doi.org/10.1016/j.measurement.2018.02.015.

[9] Nguyen, Vinh, et al. “Data-Driven Modeling of the Modal Properties of a Six-Degrees-of-Freedom Industrial Robot and Its Application to Robotic Milling.” *Journal of Manufacturing Science and Engineering*, vol. 141, no. 12, 2019, https://doi.org/10.1115/1.4045175.

[10] Verl, Alexander, et al. “Robots in Machining.” *CIRP Annals*, vol. 68, no. 2, 2019, pp. 799–822., https://doi.org/10.1016/j.cirp.2019.05.009.

[11] Sortino, M., et al. “Compensation of Geometrical Errors of CAM/CNC Machined Parts by Means of 3D Workpiece Model Adaptation.” *Computer-Aided Design*, vol. 48, 2014, pp. 28–38., https://doi.org/10.1016/j.cad.2013.10.010.

[12] Cvitanic, Toni, et al. “Pose Optimization in Robotic Machining Using Static and Dynamic Stiffness Models.” *Robotics and Computer-Integrated Manufacturing*, vol. 66, 2020, p. 101992., https://doi.org/10.1016/j.rcim.2020.101992.

[13] Altintas, Y., and M.R. Khoshdarregi. “Contour Error Control of CNC Machine Tools with Vibration Avoidance.” *CIRP Annals*, vol. 61, no. 1, 2012, pp. 335–338., https://doi.org/10.1016/j.cirp.2012.03.132.

[14] Khoshdarregi, Mohammad R., et al. “Integrated Five-Axis Trajectory Shaping and Contour Error Compensation for High-Speed CNC Machine Tools.” *IEEE/ASME Transactions on Mechatronics*, vol. 19, no. 6, 2014, pp. 1859–1871., https://doi.org/10.1109/tmech.2014.2307473.

[15] Zhang, Ke, et al. “Pre-Compensation of Contour Errors in Five-Axis CNC Machine Tools.” *International Journal of Machine Tools and Manufacture*, vol. 74, 2013, pp. 1–11., https://doi.org/10.1016/j.ijmachtools.2013.07.003.

[16] Schraeder, Travis F., and Rida T. Farouki. “Experimental Performance Analysis of an Inverse Dynamics CNC Compensation Scheme for High-Speed Execution of Curved Toolpaths.” *The International Journal of Advanced Manufacturing Technology*, vol. 73, no. 1-4, 2014, pp. 195–208., https://doi.org/10.1007/s00170-014-5720-z.

[17] Yuan, Lei, et al. “A Review on Chatter in Robotic Machining Process Regarding Both Regenerative and Mode Coupling Mechanism.” *IEEE/ASME Transactions on Mechatronics*, vol. 23, no. 5, 2018, pp. 2240–2251., https://doi.org/10.1109/tmech.2018.2864652.

[18] Kim, Seong Hyeon, et al. “Robotic Machining: A Review of Recent Progress.” *International Journal of Precision Engineering and Manufacturing*, vol. 20, no. 9, 2019, pp. 1629–1642., https://doi.org/10.1007/s12541-019-00187-w.

[19] Taylor, Russell H., et al. “Medical Robotics and Computer-Integrated Surgery.” *Springer Handbook of Robotics*, 2016, pp. 1657–1684., https://doi.org/10.1007/978-3-319-32552-1_63.

[20] Wang, Ben. “The Future of Manufacturing: A New Perspective.” *Engineering*, vol. 4, no. 5, 2018, pp. 722–728., https://doi.org/10.1016/j.eng.2018.07.020.

[21] Azadeh, Kaveh, et al. “Robotized and Automated Warehouse Systems: Review and Recent Developments.” *Transportation Science*, vol. 53, no. 4, 2019, pp. 917–945., https://doi.org/10.1287/trsc.2018.0873.

[22] Wang, Wei, et al. “Error Compensation of Industrial Robot Based on Deep Belief Network and Error Similarity.” *Robotics and Computer-Integrated Manufacturing*, vol. 73, 2022, p. 102220., https://doi.org/10.1016/j.rcim.2021.102220.

[23] Usop, Zuriani, et al. “Measuring of Positioning, Circularity and Static Errors of a CNC Vertical Machining Centre for Validating the Machining Accuracy.” *Measurement*, vol. 61, 2015, pp. 39–50., https://doi.org/10.1016/j.measurement.2014.10.025.

[24] Slavkovic, Nikola R., et al. “A Method for off-Line Compensation of Cutting Force-Induced Errors in Robotic Machining by Tool Path Modification.” *The International Journal of Advanced Manufacturing Technology*, vol. 70, no. 9-12, 2013, pp. 2083–2096., https://doi.org/10.1007/s00170-013-5421-z.

[25] Cordes, Marcel, and Wolfgang Hintze. “Offline Simulation of PATH Deviation Due to Joint Compliance and Hysteresis for Robot Machining.” *The International Journal of Advanced Manufacturing Technology*, vol. 90, no. 1-4, 2016, pp. 1075–1083., https://doi.org/10.1007/s00170-016-9461-z.

[26] Gao, Yuan-yuan, et al. “Tool Path Planning and Machining Deformation Compensation in High-Speed Milling for Difficult-to-Machine Material Thin-Walled Parts with Curved Surface.” *The International Journal of Advanced Manufacturing Technology*, vol. 84, no. 9-12, 2015, pp. 1757–1767., https://doi.org/10.1007/s00170-015-7825-4.

[27] Huang, Nuodi, et al. “Error Compensation for Machining of Large Thin-Walled Part with Sculptured Surface Based on on-Machine Measurement.” *The International Journal of Advanced Manufacturing Technology*, vol. 96, no. 9-12, 2018, pp. 4345–4352., https://doi.org/10.1007/s00170-018-1897-x.

[28] Li, Zhou-Long, et al. “Surface Form Error Prediction in Five-Axis Flank Milling of Thin-Walled Parts.” *International Journal of Machine Tools and Manufacture*, vol. 128, 2018, pp. 21–32., https://doi.org/10.1016/j.ijmachtools.2018.01.005.

[29] Sun, Yuwen, and Shanglei Jiang. “Predictive Modeling of Chatter Stability Considering Force-Induced Deformation Effect in Milling Thin-Walled Parts.” *International Journal of Machine Tools and Manufacture*, vol. 135, 2018, pp. 38–52., https://doi.org/10.1016/j.ijmachtools.2018.08.003.

[30] Kolluru, Kiran, et al. “A Solution for Minimising Vibrations in Milling of Thin Walled Casings by Applying Dampers to Workpiece Surface.” *CIRP Annals*, vol. 62, no. 1, 2013, pp. 415–418., https://doi.org/10.1016/j.cirp.2013.03.136.

[31] Nguyen, Vinh, et al. “Active Vibration Suppression in Robotic Milling Using Optimal Control.” *International Journal of Machine Tools and Manufacture*, vol. 152, 2020, p. 103541., https://doi.org/10.1016/j.ijmachtools.2020.103541.

[32] Timošenko Stepan P., and S. Woinowsky-Krieger. *Theory of Plates and Shells*. McGraw-Hill, 1996.

[33] Kline, W.A., et al. “The Prediction of Cutting Forces in End Milling with Application to Cornering Cuts.” *International Journal of Machine Tool Design and Research*, vol. 22, no. 1, 1982, pp. 7–22., https://doi.org/10.1016/0020-7357(82)90016-6.